Solar thermal powered Organic Rankine Cycles

16

M. Orosz[1], R. Dickes[2]
[1]Massachusetts Institute of Technology, Cambridge; [2]University of Lige, Lige, Belgium

16.1 Introduction to solar Organic Rankine Cycle systems

Sunlight is the primordial energy source for most of the work that has occurred on Earth in the past 4.54 billion years. The most basic transformations are physical, e.g., sunlight evaporates water from oceans, raising it into the atmosphere and transporting it hundreds of miles to fuel global precipitation patterns. The original mechanism for converting sunlight into electro-mechanical work, however, was developed by single celled organisms, probably the progenitors of today's chloroplasts. Photosynthesis, the reduction of atmospheric carbon dioxide mediated by water and light, produced oxygen (a by-product) and energy to power cellular functions, such as DNA transcription, organelle formation, metabolism, and cell division. Over time this sunlight-powered work filled the earth's atmosphere with oxygen, creating an atmosphere similar to today's, by around 2.3 billion years ago.

In the human era, the earliest references that lay a foundation for the concept of converting sunlight into work involve a compilation of two ancient Sicilian/Greek innovations. Though likely apocryphal, the AD 2nd Century author, Lucian, reported that during the Siege of Syracuse (214−212 BC), Archimedes defended the city by setting fire to Roman ships using mirrors in a parabolic arrangement to concentrate sunlight. Nearly three centuries later, Hero of Alexandria described a device for converting heat into work with an "aeolipile" in his *Pneumatica*. His device converted thermal energy into rotary motion by means of a radial expander using two opposing steam jets emanating from a central, spinning boiler, though it is not known whether it was ever put to productive use.

In the first story, sunlight is concentrated to create heat (the autoignition temperature of wood is around 250°C), while in the second, heat creates steam in a boiler, which then expands out of orifices at opposite tangents to create rotation. When combined in this way, these two innovations embody the essence of concentrating solar power (CSP). In the midst of the Industrial Revolution, this synthesis was finally put to practice, first by French inventor Augustin Mouchot, and later by Swedish American John Ericsson, although dates of international exhibition are Ericsson first, whose solar air engine was featured at the Centennial Exhibition in Philadelphia in 1876, followed by Mouchot at the Paris Universal Exhibition in 1878.

When the first solar power plant was commissioned in 1913 in Maedi, Egypt, it was still several decades before Chapin, Fuller, and Pearson would demonstrate a working

Organic Rankine Cycle (ORC) Power Systems. http://dx.doi.org/10.1016/B978-0-08-100510-1.00016-8

silicon photovoltaic (PV) cell (4% efficiency, at Bell Labs in 1954). The Maedi plant, designed by American engineer Frank Shuman, used five parabolic trough collectors (PTCs), each 62 m long and 4 m wide, to concentrate the sun's rays on a boiler tube supplying a 75 kW atmospheric (low-pressure) steam engine coupled to a water pump capable of lifting 22 cubic meters of Nile water per minute (American Inventor Uses Egypt's Sun for Power, 1916). Though technologically successful, Shuman's demonstration plant never gained traction due to the onset of the first World War and the widespread availability of cheap fossil fuels, however, experimentation with solar powered motors proliferated in the ensuing decades, including: the SOMOR solar pump invented by Italians Daniele Gasperini and Ferruccio Grassi in the 1940s; a 1 kW_e Solar ORC pump installed in Mali in 1966; and a 3 kW_e Solar ORC developed by Harry Zvi Tabor and Lucien Bronicki and demonstrated to the United Nations in 1961, leading to the formation of Ormat (Bronicki, 2013). The 354 MW_e combined Solar Energy Generating System plants, operating in California, starting in 1984, established the commercial feasibility of utility-scale CSP using primarily steam Rankine power blocks, creating an industry that has over 4.5 GW_e of installed capacity in 2015. Subsequently, the commercial viability of solar-driven ORCs has been explored at many scales: in 2006, a grid-connected 1 MW_e Solar ORC plant ("Saguaro") was commissioned in Red Rock, Arizona (Southwest USA) by Arizona Public Service (Canada et al., 2005b), while more recently, the focus on solar ORC systems has tended towards smaller scale, experimental systems optimized for niche applications, as discussed in Section 16.1.1.

16.1.1 Applications—grid connected power generation, desalinization, distributed power generation, cogeneration, and hybrid systems

Power from a solar ORC (SORC) can be useful in a variety of applications, from the ordinary supply of electrons via a traditional distribution grid, to islanded microgrids, to cogeneration for community or industrial use. Hybrid systems, involving other generation sources or one or more additional sources of, or uses for, thermal energy, are increasingly considered for solar ORC applications. This section highlights a range of typical uses for solar ORCs.

16.1.1.1 Grid connected power generation

There seems to be little scope for grid connected standalone solar ORC projects under the current technical and economic scenario. The 1 MW_e grid connected solar ORC, referenced in Table 16.2, is an unlikely application for deployment in the future due to the recent decline in the cost of the main competing technologies, i.e., fossil fuels and solar PV. Grid scale CSP using steam Rankine, higher temperature sCO_2, or air Brayton cycles are still being commercially explored, particularly in the case where the value of the energy produced lies in its dispatchability via thermal energy storage (TES) (for more detail see Section 16.2.3). At grid scale, in 2015, PV installs for under

USD 2/W peak whereas CSP typically has a specific cost of over USD 4/W of nameplate capacity (Orosz, 2015). The cost of CSP with TES, however, remains lower than the cost of PV with electrochemical batteries at large scales; whereas large-scale batteries for shifting PV production into the evening are commercially unavailable, TES operational experience exists at the GWh scale in several CSP plants (see Table 16.1). This indicates that a solar ORC with TES may have a role to play in meeting energy needs as a dispatchable power source in a future where the grid is comprised of a high fraction of irregular, renewable sources.

16.1.1.2 Distributed power generation

Whereas the value of dispatchability in grid connected solar power plants is only beginning to gain recognition in the market, the demand variance and the need for storage of intermittent sun power is already inherent in any load-following application such as an isolated industrial or community mini-grid. Operational experience with islanded solar ORC systems is limited and commercially immature, however, recent analyses suggest that the application of solar ORC to support energy needs in remote areas for commercial or community loads may, if properly sized and designed, be economically attractive in comparison with alternative systems capable of meeting the demand dynamic, such as diesel generators (Mitterhofer and Orosz, 2015) or PV arrays with large battery storage systems. The attractiveness of the solar ORC for distributed generation can also be increased when hybrid solutions are relevant, as discussed in Section 16.1.1.5.

16.1.1.3 Desalination

Direct solar distillation of brackish water or seawater has been practiced from an early time through the coupling of a solar collector with a traditional still. Indirect desalination, through multiple stage flash distillation or reverse osmosis (RO), utilizes solar energy to derive either solar-derived electricity or mechanical work (and potentially heat) to purify water. Investigation of solar ORC desalination has included both dual use (electricity and water) and cogeneration systems, in which the water desalination mode directly couples the ORC shaft output to a high-pressure pump feeding brackish water to an RO membrane. The feedwater in these systems can be used for heat rejection from the ORC, and the increased temperature of the water improves the efficiency of the RO (Tchanche et al., 2010; Manolakos et al., 2007; Delgado-Torres and García-Rodríguez, 2007).

16.1.1.4 Irrigation

Solar-powered ORCs can also be used for irrigation duty for agricultural production. In such systems, solar energy supplied to an ORC is converted into mechanical power which is directly exploited to drive an irrigation pump. The advantages of solar water pumping include the coincidence between seasons of high solar irradiation and the demand for irrigation, and the fact that, as a load, irrigation is relatively insensitive to the diurnal intermittency of solar power (Pytilinski, 1978).

Table 16.1 **Comparison of recently installed large-scale solar power plants using photovoltaic (PV) or concentrating solar power (CSP) technology, including specific costs and hours of storage (Orosz, 2015)**

Plant name	Type	Nameplate (MW)	Pricetag (USD 000,000)	Reported production (GWh/year)	Storage (h)	Installed cost (USD/W)	Installed cost (USD/kWh/year)
Lalackama	PV	60	110	160	0	1.83	0.69
Chañares	PV	40	70	94	0	1.75	0.74
Desert Sunlight	PV (CdTel)	550	1900	1024	0	3.45	1.86
Crescent Dunes	CSP tower	110	975	485	10	9.09	2.01
Antelope Valley	PV (CdTel)	230	1400	623	0	6.09	2.25
Topaz	PV (CdTel)	550	2400	1053	0	4.36	2.28
Agua Caliente	PV (CdTel)	290	1800	741	0	6.21	2.43
Andasol 1	CSP trough	150	380	150	7.5	2.53	2.53
Solana	CSP trough	280	2000	600	6	7.14	3.33
Ivanpah	CSP Tower	392	2200	519	0	5.61	4.24

16.1.1.5 Hybrid solar organic Rankine cycle

Solar ORCs with or without TES may be used in conjunction with a variety of other generation technologies, some of which are simply used in parallel or potentially scheduled sequentially via a macro level control strategy. Other sources of energy include PV arrays, concentrating PV/thermal (CPVT) collectors, fuel-based generator sets, fuel cells, wind turbines, biomass boilers (Fig. 16.1), waste heat recovery, geothermal, etc. A solar ORC may also be configured to bypass heat around the ORC to directly meet thermal loads, such as industrial process heat (e.g., beverage bottle cleaning, aiding flash distillation processes, enhanced oil recovery, etc.), an absorption chiller, or building heating or hot water supplies. These configurations, while involving increasing degrees of complexity, may justify the capital expense based on fuel or battery cost savings (in the case of islanded operation), increased capacity factor, and the leveraging of locally available resources.

The benefits of hybridizing solar ORC with combustion based generators include, reduced fuel consumption (replacing fuel-derived power with solar-derived power) and the potential for improved overall fuel efficiency via recuperating waste heat from the exhaust stream of the genset. Hybridizing with PV arrays can be attractive if the daytime loads are supplied via the relatively inexpensive PV, while solar thermal production is dispatched from the TES, to supply nighttime loads, displacing the need for costly batteries. CPVT with ORC represents an opportunity to further reduce the infrastructure involved in a PV−CSP hybrid.

The capital cost of CSP collectors is especially justified when local demand for heat exists, or when available waste heat is at low temperatures that could benefit from solar boosting (e.g., from server datacenters). Some industrial processes may be supplied by CSP alone without the use of an ORC, but dynamics in load and solar resource (see Section 16.3.3) will tend to create a mismatch in the availability and requirement for heat. Excess heat from the collectors can, in this case, be exploited by an ORC, offsetting plant power consumption. Similarly, in cases where the thermal loads are seasonal (e.g., wintertime heating of buildings) the addition of an ORC can

Figure 16.1 1 MW_e Shive village electrification plant (Thermax India), a hybrid plant consisting of a concentrating solar power (CSP) collector field, steam Rankine cycle, Organic Rankine Cycle, and a backup biomass-fired boiler. Left: Thermax PTC collector. Right: GE/Calnetix 100 kW_e ORC (Thakur, 2013).

productively utilize otherwise wasted summertime CSP production. Another option making use of seasonal surplus solar resource, with or without ORC, would be to integrate a multieffect absorption chiller, although the cost of this approach compared to PV driving an electric heat pump would be worth exploring. Other hybridization scenarios are possible such as combining ORC with vapor compression cooling (Dumont et al., 2015); the key considerations in selecting and specifying the solar ORC components is the value of dispatchability and thermal products, and the costs otherwise incurred via alternate solutions. This highlights the fact that hybrid solutions tend to be unique and site specific, and one must recognize that the cost of investigating each situation and engineering the integration of multiple systems, which may require novel control strategy implementations, poses an obstacle to widespread adoption.

16.1.2 Meteorological and solar resource dynamics

As noted in the introduction to this chapter, a solar ORC obtains its heat input from the sun at the center of our solar system. While the astrophysics and celestial mechanics of this star are beyond the scope of this book, a basic overview of the functionality of the solar resource and its influence on the design and optimization of thermal power systems will be summarized.

16.1.2.1 Sunlight energy

The sun is a complex thermonuclear reactor whose mass holds the earth and other solar system objects in its gravitational field, while releasing 3.86×10^{26} J/s via the fusion of hydrogen into helium. At its outermost layers, the sun surface is maintaining a temperature of approximately 5778 K. According to Planck's well-known equation for the spectral radiance of a body at thermal equilibrium at temperature T:

$$B_\lambda = \frac{2hc^2}{\lambda^5} \frac{1}{e^{\frac{hc}{\lambda k_B T}} - 1} \tag{16.1}$$

(where B is the power in Watts per m^2 per nm, λ is the wavelength, k_B is the Boltzmann constant, h is the Planck constant, and c is the speed of light in the medium) the sun emanates a constant spherical beam of electromagnetic radiation with a distinct spectral signature approximating that of a blackbody at 5778 K.

16.1.2.2 The solar spectrum

Due to the size of the earth (DIA = 12,742 km) and its distance from the sun [1.496×10^8 km or 1 astronomic unit (AU)] the amount of solar energy intercepted by the earth is 1.74×10^{17} J/s. The shape of the solar spectrum is comparable to a blackbody at 5778 K, however, the actual solar spectrum is modulated by the sun's composition and partially attenuated by absorption bands in the earth's atmosphere in proportion to the depth of atmosphere traversed by a ray emanating from the sun.

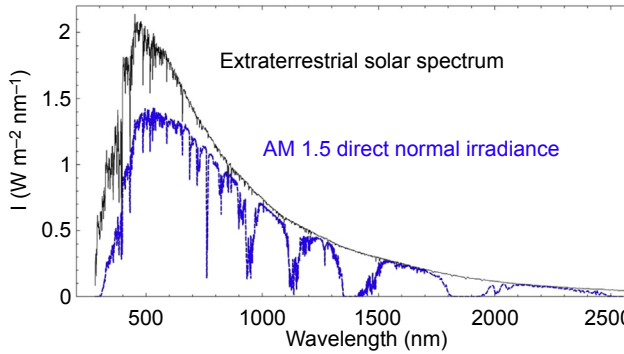

Figure 16.2 Extraterrestrial and Direct Normal Irradiance (DNI) from ASTM G173 DNI is at an air mass of 1.5 (ASTM, 2012).

Due to the rotation of the earth on an ~23.5 degrees tilted axis, this depth varies by latitude, seasonality, and time of day. The sunlight impinging on a flat plane at the surface of the earth is nearly collimated (the sun shape has an acceptance angle of 0.55 degrees); the intersection of a spherical beam of sunlight projected out from the sun across 1 AU distance striking the earth results in an extraterrestrial *solar constant* of approximately 1367 W/m^2. An approximation of the direct normal irradiance (DNI—the beam component as opposed to diffuse light) solar spectrum at 1.5 times the thickness of the atmosphere is a frequently used standard for CSP known as AM1.5D (where D stands for direct, shown in Fig. 16.2). At prospective CSP sites, historical DNI measurements, obtained with a pyrheliometer, can be used to estimate local solar resources.

While the detailed characteristics of the solar spectrum have implications for the optical performance of solar collectors (specular reflectivity of primary mirrors, absorption, etc.), it is not uncommon to simply deploy the integral of the spectrum (in W/m^2), as a ready means of ascertaining power flux impinging on a collector aperture. The solar constant at the top of the atmosphere (~1367 W/m^2) is reduced by 25% or more by atmospheric conditions; at high DNI locations, at the earth's surface, it can reach above 1000 W/m^2 and 7.5 kWh/m^2/day. A more typical range for areas still considered appropriate for use of CSP is above 800 W/m^2 and 5 kWh/m^2/day, and standards or specifications for collector output will typically specify the DNI conditions at which the measurements were made.

16.1.2.3 Tracking

Most CSP collectors employ imaging optics that require the aperture of the collector to be normal to the sun. From dawn until dusk the sun is constantly moving in azimuth and zenith (zenith is 90-elevation, where elevation is the angle between the horizon and the sun) with respect to a fixed location on a rotating earth. Point focus systems, unlike line-focus systems (both described further in Section 16.2.1) must move to track the sun position in both azimuth and zenith coordinates (known as A-Z tracking).

In line-focus systems 2-D tracking is possible, however, the more common approach is the minimization of the cosine of the angle ϕ (between the collector aperture and the sun) by means of tracking around a single north-south or east-west axis. Compared to a horizontal surface, the increased solar irradiance on a single-axis tracking surface is approximately 10−20% or 20−30% for east-west and north-south parallel axes respectively, depending on latitude, with an additional 5−10% possible for two-axis tracking (Helwa et al., 2000; Duffie et al., 1994). Algorithms for calculating the sun position (azimuth and elevation) as a function of latitude, longitude, and time are published by National Renewable Energy Laboratory (NREL) in the USA and the Plataforma Solar de Almería (PSA) in Spain Reda and Andreas, 2008). Calculating the tilt angle for a single-axis platform in an east-west or north-south orientation CSP system involves minimizing the angle of incidence between the collector and impinging sunlight; equations for obtaining this result are widely available in the literature (Duffie et al., 1994).

16.1.2.4 Intermittency

ORCs driven by geothermal or waste heat sources can usually be designed with near constant heat input rates, or rates that vary in a predictable and controllable manner. ORCs driven exclusively or partially via solar input must contend with thermal inputs that can vary with unknown frequency and magnitude, superimposed on other fluctuations with a wide range but having a greater degree of predictability. Solar concentrators (discussed in more detail in Section 16.2), experience varying intensity of sunlight on their aperture on the timescale of seconds to minutes during cloud passing, on the timescale of hours due to the diurnal cycle, and on seasonal timescales on the basis of latitude driven changes in the time varying pathlength of rays through the atmosphere (as well as any attending angle of incidence effects). Landscape shadowing effects can have both diurnal and seasonal components. The DNI on a single-axis tracking surface for a typical cloudless day is shown in Fig. 16.3 and it is contrasted to cloudy weather at the same location; the effect of cloud passing can be seen to produce rapid changes in energy flux that require further design considerations when coupling CSP and ORC technologies (see Section 16.2.3).

16.1.2.5 Solar resource maps

The spatial distribution of the availability of beam (relatively collimated) sunlight (i.e. DNI), versus global irradiance (DNI + diffuse light) on an average daily basis (integrating the fluctuations due to local weather) per square meter for locations on earth's surface has been characterized by a combination of ground based and satellite measurements to produce useful maps for planning solar projects, an example of which is shown in Fig. 16.4:

For a more granular representation of local conditions, Typical Meteorological Year (TMY) datasets that include pryheliometer measurements (for measuring DNI) are particularly useful for simulating the dynamic behavior of solar systems (discussed in more detail in Section 16.3.3).

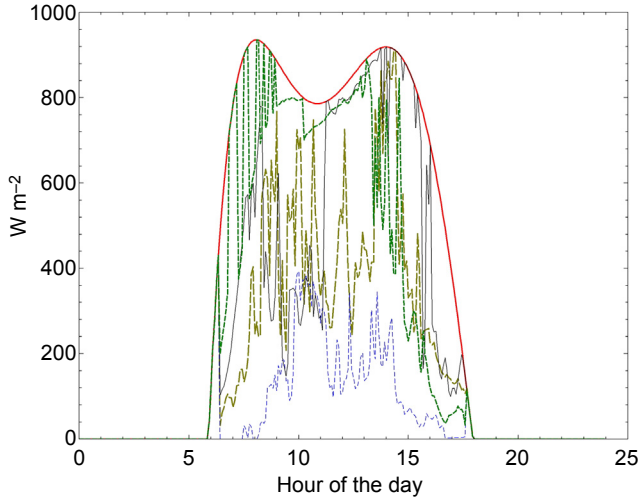

Figure 16.3 DNI on a single-axis tracking surface (Lesotho, 2009) for a cloudless day (red) and various cloudy days.
Adapted from Ireland et al. (2014).

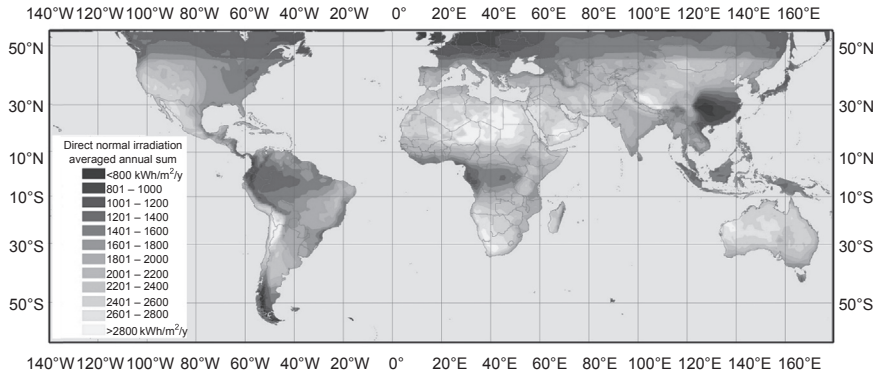

Figure 16.4 Map of direct normal irradiance (DNI) at the earth's surface in kWh per square meter annually.
Adapted from NASA SSE 6.0 (1993–2006) and DLR (2008).

16.1.3 Installed capacity—survey of existing sites

Since the first development of heat engines, solar energy has been considered as a viable heat source. While none of the earliest experimental investigations of solar-based ORCs are in existence today, records and examples of experimental power plants are available, including unique pilot systems for R&D and commercial power generation units built and tested in the 20th century to the present. These SORC facilities range from "micro-power" generation (typically defined as lower than 1 MW_e) to large power plants of several megawatts, representing many variants of the technology.

The records for these systems are incomplete, but an effort to compile a list of known plants was undertaken by Mueller et al. (2016) and from this dataset of diverse solar-based ORC systems, a nonexhaustive list of experimental and commercial power plants with known characteristics is provided in Table 16.2.

16.2 Solar Organic Rankine Cycle components and architecture

16.2.1 Solar thermal collectors

Solar-based ORCs use solar energy as the heat source from which to generate electricity or mechanical power. The heat is obtained by means of solar thermal collectors which intercept incoming sunlight and collect or reflect it onto a heat collection element (HCE). At the HCE, light is converted to sensible or latent heat and typically transferred to a flowing transport medium, called the heat transfer fluid (HTF). In most situations, the HTF acts an intermediate fluid that transports heat to the ORC evaporator, however, direct generation can also be performed if the ORC working fluid is circulated through the HCE in place of a separate HTF, as discussed in Section 16.2.2. The thermal efficiency of solar collectors depends significantly on the operating conditions and the insulation quality of the HCE, with values for the thermal efficiency typically ranging from 30% to 70%. For an HCE, the higher the temperature difference between the ambient air and the HCE, the higher the thermal losses.

Many types of thermal collectors have been developed in past decades and a major distinction can be made between concentrating and nonconcentrating technologies. A nonconcentrating collector has the same surface area for intercepting (aperture) and for absorbing (HCE surface) sunlight (the radiation flux onto the HCE is not increased), and a tracking system is not usually required. Both direct and diffuse portions of sunlight are exploited, and non-concentrating collectors can be well-suited for low-temperature applications. In the case of solar-based ORCs, three main technologies are used, namely solar ponds, flat plate collectors, and evacuated tube collectors.

16.2.1.1 Salt-gradient solar pond

A salt-gradient solar pond (SGSP), or simply *solar pond*, is a pool of saltwater used for collecting solar energy. Within the reservoir, a vertical salt concentration profile creates a three-layer stratification dividing the brine into an upper convective zone (UCZ) at the surface, a nonconvective zone (NZC) in the middle, and a lower convective zone (LCZ) at the bottom (see Fig. 16.5). While the top and bottom zones have a quasi-uniform density (low and high respectively) the nonconvective zone features a density profile that increases continuously from the upper to the lower boundary. As such, any natural convection is eliminated in the middle zone and a stable insulation layer is formed. During sunny periods, solar radiation passes through the layers and is absorbed by the lower zone. Thanks to the stable intermediate layer (NCZ in Fig. 16.5), the temperature of the bottom zone rises (up to 95°C) whereas the top of

Table 16.2 Nonexhaustive review of existing experimental solar Organic Rankine Cycle (SORC) facilities

Location (date)	Collector technology[a]	Collector area	Heat transfer fluid	Power output	Working fluid	Thermal storage	References
Mali (1966)	FPC	43 m^2	–	600 W	–	None	Einav (2004)
Ein Bokek, Israel (1977)	SGSP	7000 m^2	Brine	150 kW	–	Solar pond	Tabor (1981)
Pasadena, CA - USA (1978)	PDC	116.9 m^2	Toluene	30 kW	Toluene	None	Kiceniuk (1985)
Willard, NM - USA (1979)	PTC	1276 m^2	Mineral oil	19 kW	R113	Thermocline direct	Fenton et al. (1984)
Kuwai city, Kuwait (1981)	PDC	1100 m^2	Synthetic oil	100 kW/ 700 kW_{th}	Toluene	Thermocline direct	Moustafa et al. (1984)
Vignola, France (1982)	PTC	1176 m^2	Thermal oil	100 kW	Fluoroinert FC75	Thermocline direct	Simonnot et al. (1987)
Perth, Australia (1984)	PTC	–	Thermal oil	35 kW	C_8F_{16}	–	Barutti et al. (1984) and Bado et al. (1979)
Beith Ha'Arava, Israel (1982)	SGSP	250,000 m^2	Brine	5 MW	–	Solar pond	Tabor and Doron (1990)
Lausanne, Switzer (2001)	LFC	100 m^3	Water	15 kW	R123/R134a	None	Kane et al. (2003)
Sendai, Japan (2002)	CPC	5.75 m^2	Water	<1 kW	R113	Buffer	Saitoh et al. (2007)
Red Rock, AZ–USA (2006)	PTC	10340 m^2	Mineral oil	1 MW	n-pentane	None	Canada et al. (2005a)
Newcastle, Australia (2006)	PTC	132 m^2	Mineral oil	6 kW	HFE 7100	n.a.	Kohlenbach et al. (2006)
Almeria, Spain (2007)	PTC	n.a.	Thermal oil	5 kW	SES36	n.a.	Galvez (2010)

Continued

Table 16.2 Continued

Location (date)	Collector technology[a]	Collector area	Heat transfer fluid	Power output	Working fluid	Thermal storage	References
Tianjin, China (2008)	FPC	0.6 m^2	R245fa	13 W	R245fa	None	Wang et al. (2011)
Tianjin, China (2008)	FPC/ETC	44 m^2	R245fa	1.7 kW	R245fa	None	Wang et al. (2010)
Morphou, Cyprus (2010)	PTC	216 m^2	Water	18 kW	R245fa	n.a.	Electratherm (2010)
Burkina Faso (2012)	SCT	180 m^2	Mineral oil	10 kW	R245fa	Two-tank direct	N'Tsoukpoe et al. (2014)
Berea, Lesotho (2012)	PTC	75 m^2	Glycol	3 kW/ 25kWth	R245fa	n.a.	Orosz (2012)
Crowley, LA−USA (2013)	PTC	1051 m^2	Water	50 kW	R245fa	Buffer	Chambers et al. (2014)
Tampa, FL−USA (2013)	PTC	n.a.	Water/ ethylene	50 kW	R245fa	PCM	Goswami et al. (2013)
Cadarache, France (2013)	PTC	550 m^2	Water	10 kW	R245fa	Thermocline direct	Rieu (2012)
Ait-Baha, Morocco (2014)	PTC	6159 m^2	Air	3 MW	n.a.	Sensible packed-bed	Ait-Baha
Rende, Italy (2014)	LFC	9780 m^2	Mineral oil	1 MW	n.a.	None	NREL
Fallon, NV−USA (2015)	PTC	656 m^2	Water	33 MW	Isobutane	None	NREL
Liège, Belgium (2015)	PTC	78 m^2	Synthetic oil	3 kW	R245fa	None	Georges et al. (2013) and Dickes et al. (2014)
Busan, Korea (2015)	ETC	n.a.	Water	1.5 kW	R245fa	n.a.	Baral et al. (2015)

[a]*CPC*, compound parabolic collector; *ETC*, evacuated tube collector; *FPC*, flat plate collector; *LFC*, linear Fresnel collector; *PDC*, parabolic dish collector; *PTC*, parabolic trough collector; *SCT*, solar central tower; *SGSP*, salt-gradient solar pond.

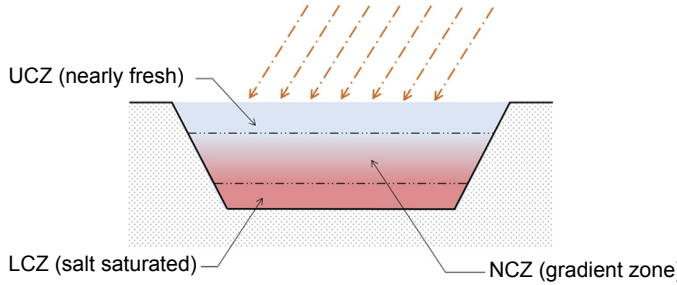

Figure 16.5 Salt-gradient solar pond. LCZ, lower convective zone; *NCZ*, nonconvective zone; *UCZ*, upper convective zone.

the pond remains close to the ambient temperature. Depths of solar ponds range from 0.5 to 5 m and large surface areas are required (>200,000 m^2) for powering large-scale systems. Thermal energy is transferred to the ORC by pumping some of the hot brine to the evaporator and the upper cold water can be used as a heat sink for the ORC condenser. A key advantage of solar ponds is their ability to both collect and store thermal energy. Thanks to the high thermal inertia of the reservoir, heat power can be delivered to the ORC at a stable temperature.

16.2.1.2 Flat plate collector

A flat plate collector (FPC) is made of fluid tubes (filled with flowing HTF) connected to a darkened (high absorptivity) flat plate absorber that collects the sunlight and transfers the heat energy to the tubes. To reduce both convection and radiation losses, a transparent cover protects the absorber, while conduction losses are limited with an efficient thermal insulation of the collector casing. An example FPC architecture is shown in Fig. 16.6. Initially designed for domestic hot water generation, this technology is well-suited for low-temperature applications (below 100°C) and achieves good thermal efficiencies thanks to the limited heat losses.

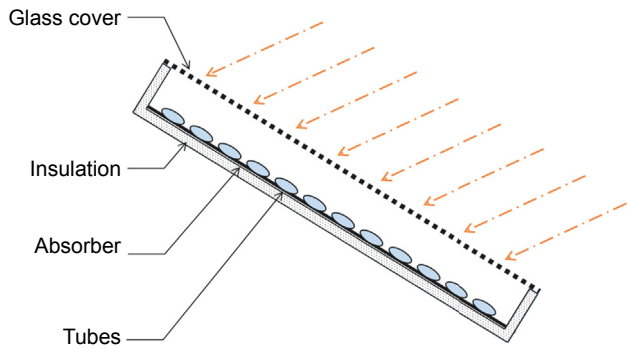

Figure 16.6 Flat plate collector.

16.2.1.3 Evacuated tube collector

To decrease heat losses at high temperature or in unfavorable weather conditions, an evacuated tube can be placed around the HCE of a solar collector. Evacuated tube collectors (ETC) can be found in two different configurations: in the first, the HTF flows directly through the tube placed in the middle of the evacuated envelope while in the second configuration, as depicted in Fig. 16.7, a heat pipe is placed in the vacuum-sealed tube and an auxiliary phase-change medium is used to transfer solar energy to the main HTF by means of an evaporation−condensation cycle. More precisely, solar radiation evaporates the auxiliary medium, after which the vapor phase naturally migrates to a condenser situated at the top of the heat pipe. The heat energy is then transferred to the main HTF, and the cooled auxiliary medium flows down the heat pipe in liquid phase. Although more complex, this mechanism permits collection of solar energy at constant temperature and avoids issues with overheating or freezing. Like flat plate collectors, ETCs exploit both direct and diffuse solar radiation, but ETCs have better thermal performance than FPCs for similar operating conditions and are suitable for a somewhat higher temperature range (up to 150°C).

In many cases, however, it is desirable to operate solar collectors at temperatures above even 150°C, and this requires use of a concentrating collector (using mirrors or lenses to focus sunlight) to increase the flux density at the HCE. Concentrating collectors therefore have a larger aperture area than HCE area, and the ratio between these two surfaces is known as the concentration ratio (C_f). Depending on the technology, the concentration ratio can be slightly larger than one or reach over one thousand. At a given operating temperature, the higher the concentration ratio, the higher the thermal efficiency. The heat loss from an HCE of a given surface area and optical properties is proportional to the average temperature difference between the HCE and the ambient environment. Therefore, for a given operating condition, the efficiency increases with the concentration ratio C_f since the losses are reduced in proportion to the heat input. Solar collectors can be designed and operated to achieve high temperatures for the heat source and thus a better thermodynamic efficiency of the ORC. Note, however, that a tradeoff must be made for this efficiency gain, as higher

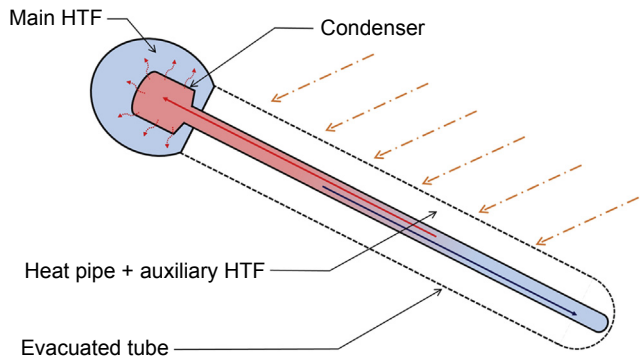

Figure 16.7 Evacuated tube collector.

temperatures at the HCE also increase thermal losses of the collector. Unlike non-concentrating technologies, concentrating collectors usually require continuous tracking to ensure an efficient focus of incoming radiation onto the HCE, and their optical imaging nature means they exploit only DNI and demonstrate poor performance in diffuse solar conditions. The most common concentrating technologies employed in SORC are presented in the following Sections 16.2.1.4–8.

16.2.1.4 Parabolic trough collector

A parabolic trough collector (PTC) is a linear concentrating system made of long, parabolic-shaped mirrors and a receiver tube placed along the focal axis of the parabola. DNI is concentrated onto the receiver tube (as illustrated in Fig. 16.8), where solar energy is absorbed by the HTF. A glass envelope is often placed around the HCE to limit convection losses and further improve the collector efficiency; the annulus space between the glass envelope and the receiver tube can be under vacuum. Common PTCs achieve concentration ratios of 50, and the HTF temperature can reach up to 400°C (Lovegrove and Stein, 2012). Parabolic troughs are highly modular and can be arranged in solar fields of various sizes and architecture, however, to minimize losses, the collector axis must be oriented either in an east-west or in a north-south direction, both of which require single-axis tracking. In the case of a smaller solar field, dual-axis tracking can be used to reduce optical losses, however, this is relatively uncommon for linear concentrators.

16.2.1.5 Linear Fresnel collector

A linear Fresnel collector (LFC) is a line-focused concentrating system that reflects DNI onto an elevated stationary receiver tube (see Fig. 16.9). Unlike PTCs which consist of a continuous parabola-shaped reflector, LFCs are composed of many long strips of mirror that can be moved independently (single-axis tracking) to achieve reflection of solar radiation onto the HCE. Due to its architecture, LFCs are highly modular and can be constructed and assembled inexpensively in various-scale solar

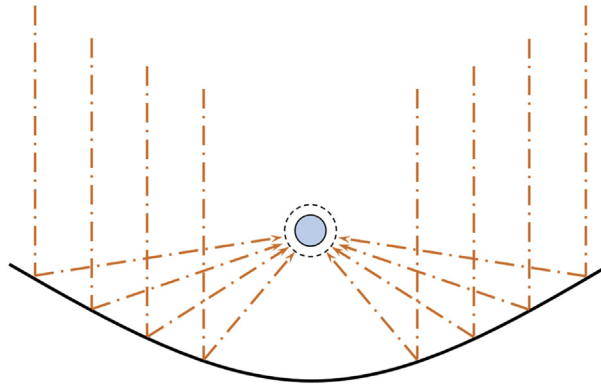

Figure 16.8 Parabolic dish/trough collectors.

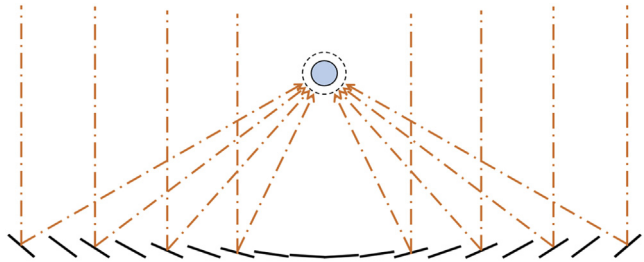

Figure 16.9 Linear Fresnel collector.

fields. Concentration ratios of LFCs without secondary optics are slightly lower than for PTCs, and LFCs are generally characterized by lower optical performance but potential cost savings.

16.2.1.6 Compound parabolic collector

A compound parabolic collector (CPC) (see Fig. 16.10) is another trough-type technology that concentrates solar energy onto a tube receiver. The reflector geometry is built by the combination of two symmetric parabolic segments with different focal lengths. This geometrical arrangement enables collection of any solar radiation entering the collector aperture within an acceptance angle (depending on geometry but ranging from 10 to 80 degrees) onto the tube receiver by means of multiple internal reflections. This important feature allows CPCs to operate without continuous tracking and to exploit both DNI and some portions of diffuse sunlight. CPCs are characterized by low concentration ratios (<5) and are well-suited for medium-temperature applications (up to 200°C). CPCs also find use as secondary down-facing reflectors in LFC systems to increase the effective concentration ratio.

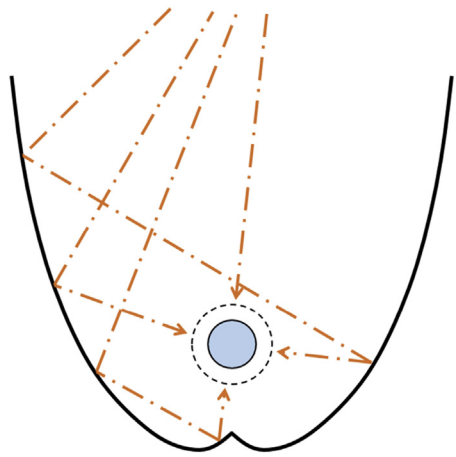

Figure 16.10 Compound parabolic collector.

16.2.1.7 Parabolic dish reflector

A parabolic dish reflector (PDR) is a point-focus system with a paraboloid geometry given by the revolution of one half of a parabola around its normal axis. Sunlight entering the collector aperture with a normal incidence is concentrated onto a heat receiver located at the focal point of the dish. Parabolic dishes exploit only DNI and require a two-axis tracking mechanism to ensure a proper focus throughout the day. Typical concentration ratios of PDRs range from 500 to 3000, making this technology suitable for high temperature applications (up to 450°C for SORCs), but unlike other collector types, PDRs are rarely connected together in a solar field. Instead, they often operate as distributed power systems with independent engine units directly located at the focal point of each collector. Due to their high temperature capabilities, ORC is not often the cycle of choice for a PDR collector, with Stirling and thermoacoustic examples being more common (Kiceniuk, 1985; Dfid, 2010; Zhang et al., 2014).

16.2.1.8 Solar central tower

A solar central tower (SCT) is another type of point-focus system that uses a field of independently actuated mirrors (called heliostats) to concentrate DNI onto a central receiver at the top of a tower (Fig. 16.11). Each heliostat is controlled with a 2D tracking mechanism calibrated to its location and physical placement relative to the tower. Solar towers achieve high concentration ratios (up to 2000) and are most often used in high-temperature large-scale steam power plants, however, some pilot projects (see Table 16.2) also use this collector technology in ORC-based power systems.

The selection of an appropriate solar collector technology for an ORC application will involve specific cost considerations, or the comparison of alternatives, along with project specifications including any limitations in mounting space, operating temperatures, and the availability of any reservoir for heat rejection (discussed further in Section 16.3.4). The main characteristics of the different collector technologies presented in this section are summarized in Table 16.3.

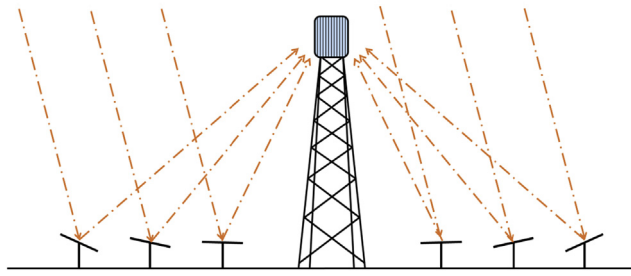

Figure 16.11 Solar tower system with heliostat array and central receiver.

Table 16.3 Solar collectors used in solar Organic Rankine Cycles (SORCs) and their characteristics (Lovegrove and Stein, 2012; Kalogirou, 2004; Weinrebe, 2007)

Collector type	SGSP	FPC	ETC	CPC	LFC	PTC	PDR	SCT
Tracking	None	None	None	None/1D	1D	1D/2D	2D	2D
Concentration ratio	1	1	1	<5	20–40	30–50	500–3000	400–2000???
Solar exploitation	Total	Total	Total	Total	Direct only	Direct only	Direct only	Direct only
Receiver temperature	<100°C	<100°C	100–150°C	100–200°C	100–300°C	100–400°C	>300°C	>300°C

CPC, compound parabolic collector; *ETC*, evacuated tube collector; *FPC*, flat plate collector; *LFC*, linear Fresnel collector; *PDR*, Parabolic dish reflector; *PTC*, parabolic trough collector; *SCT*, solar central tower; *SGSP*, salt-gradient solar pond.

16.2.2 Heat transfer fluid

In general, a flowing heat carrier fluid (HTF) is used to facilitate transfer of energy collected in the solar field to the ORC unit.

A simpler option is to directly use the working fluid of the organic Rankine cycle as the heat transport medium (Fig. 16.12 left side), referred to as *direct steam generation* (DSG), vaporizing the organic fluid within the solar collectors. This configuration avoids the cost of a heat delivery heat exchanger and the parasitic losses associated with a pump circulating a second fluid, and the simple architecture makes it convenient for use in micro-scale systems (Lovegrove and Stein, 2012). DSG is rarely utilized in medium- and large-scale SORC systems due to the large (costly) volume of organic fluid required to fill the solar field; DSG implies high-pressure operations in the solar collectors which requires a more expensive collector design and may actually increase the overall cost of the project.

The second, more common, SORC architecture employs an intermediate HTF to transport collected heat energy from the solar collectors to the ORC system. In this case, a heat exchanger between the solar loop and the ORC is used to evaporate the working fluid (heat delivery similar to that used in more traditional ORC applications), and a secondary pump circulates the HTF in the solar collectors.

The selection of an efficient and cost-effective HTF is one of the important design parameters affecting the overall power plant performance. The main solar plant HTF requirements are summarized here:

1. Low melting temperature, to avoid solidification and an adequate pumpability of the HTF during cold weather;
2. High temperature stability, to ensure the HTF integrity at high-temperature operating conditions;
3. High thermal conductivity, to maximize the heat transfer rate in the solar collectors;
4. High thermal capacity, to limit the mass flow rate required for transporting a given amount of heat power;
5. Low coefficient of expansion, to limit the volume variations of the HTF between different operating conditions;
6. Low viscosity, to reduce power consumption of circulating pumps;

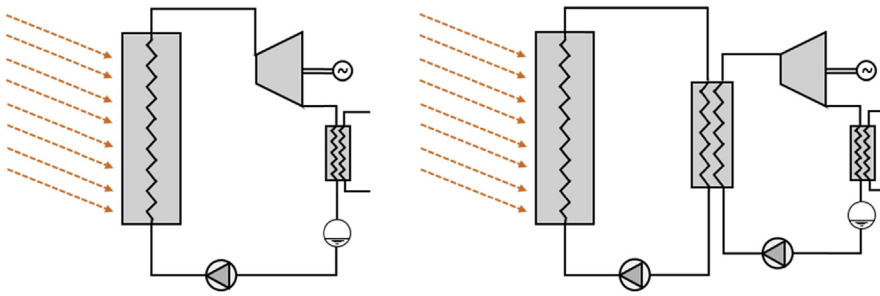

Figure 16.12 Direct steam generation (DSG) configuration (left). Heat transfer fluid (HTF) configuration (right).

7. Low corrosion, to ensure the long-term integrity of the power plant;
8. Limited hazard and environmental issues, i.e., low vapor pressure, no toxicity, limited flammability, etc.;
9. Low cost and availability within the project target market.

A common, effective, and inexpensive heat carrier used in low-medium temperature SORC is pressurized water. Aside from low cost, wide availability, and the absence of environmental issues, water has good heat transfer properties with a low viscosity and a high thermal capacity. A major drawback of water, however, is the sharp increase of pressure required to ensure a liquid-phase flow at high temperature, as shown in Fig. 16.13. Pressures in water-based solar fields easily reach 20 bar, making the installation more hazardous (from a mechanical safety perspective) and more expensive. Working HTF pressure can become a limiting factor in solar field operating temperature, which limits in turn the maximum temperature of the working fluid inside the ORC.

Low-pressure operations in the solar field can be preserved by admixture of water with soluble fluids that lower the boiling point, such as the glycol diols, or using alternative fluids such as thermal oils or other organic or inorganic materials. These HTFs can be vegetal (e.g., palm oil), synthetic (i.e., artificially-made), mineral (i.e., petroleum-derived), or liquefied salts; HTFs of these types have been developed for use in a wide range of temperature ranges and conditions (see Table 16.4). It is important to recall that HTF properties are generally temperature dependent; Table 16.4 provides one point of comparison among fluids (at 150°C) and the coefficients required to calculate the density and the specific heat capacity of the fluids in function of the temperature, i.e.,

$$\rho_T = \rho_0 + \beta_\rho T \quad cp_T = cp_0 + \beta_{cp} T \tag{16.2}$$

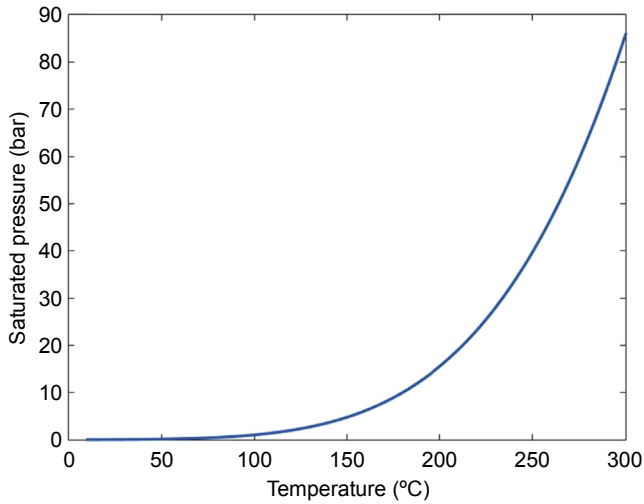

Figure 16.13 Saturated pressure of water as a function of the temperature.

Table 16.4 Nonexhaustive list of range of commercial heat transfer fluids (HTFs)

Fluid	T_{min}	T_{max}	$T_{auto,ig}$	$\rho_{150°C}$	$cp_{150°C}$	$k_{150°C}$	$\mu_{150°C}$	ρ_0	β_ρ	cp_0	β_{cp}
	(°C)	(°C)	(°C)	(kg/m^3)	(J/kg K)	(W/m K)	(cP)	(kg/m^3)	(kg/m^3 °C)	(J/kg K)	(J/kg K °C)
Water (20 bar)	–	–	–	**918**	**4302**	**0.682**	**0.18**	**1024**	**−0.725**	**4099**	**1.49**
Xceltherm 600	−29	316	349	773	2440	0.126	1.07	864	−0.607	1927	3.41
Xceltherm MK1	12	400	621	957	1916	0.121	0.59	1093	−0.942	1495	2.77
Xceltherm LV1	7	371	604	955	1944	0.120	0.70	1080	−0.835	1519	2.79
Dynalene MT	–	350	410	862	2083	0.118	1.10	972	−0.732	1772	1.72
Dynalene HT	−34	350	450	951	2033	0.113	1.51	1058	−0.715	1474	3.73
Dynalene SF	−60	315	330	789	2441	0.124	1.66	890	−0.672	1906	3.60
Dynalene SGXT	−27	176	n.a.	931	7863	0.433	7.51	1054	−0.640	3445	5.83
Dynalene 600	−65	288	n.a.	833	1517	0.130	17.00	983	−1.000	1234	1.88
Therminol 66	−3	345	399	921	2014	0.110	1.52	1028	−0.735	1475	3.65
Therminol XP	−29	315	324	795	2394	0.117	1.48	893	−0.668	1747	4.13
Therminol 59	−61	315	404	878	2110	0.110	0.74	990	−0.771	1614	3.32
Therminol 55	−54	315	343	783	2364	0.113	1.29	887	−0.705	1836	3.53
Therminol SP	−40	315	366	783	2368	0.113	1.29	888	−0.716	1836	3.54
Therminol 62	−42	325	407	859	2252	0.111	1.06	973	−0.794	1907	2.15
Therminol VP1	12	400	621	957	1913	0.121	0.59	1098	−0.972	1486	2.82
Dowtherm A	12	400	599	952	1940	0.118	0.58	1096	−0.995	1501	2.93
Dowtherm G	4	360	432	946	2000	0.111	0.96	1062	−0.775	1476	3.50
Dowtherm Q	−35	330	412	867	2058	0.104	0.45	981	−0.758	1596	3.03

Continued

Table 16.4 Continued

Fluid	T_{min}	T_{max}	$T_{auto,ig}$	$\rho_{150°C}$	$cp_{150°C}$	$k_{150°C}$	$\mu_{150°C}$	ρ_0	β_ρ	cp_0	β_{cp}
	(°C)	(°C)	(°C)	(kg/m^3)	(J/kg K)	(W/m K)	(cP)	(kg/m^3)	(kg/m^3 °C)	(J/kg K)	(J/kg K °C)
Water (20 bar)	–	–	–	**918**	**4302**	**0.682**	**0.18**	**1024**	**−0.725**	**4099**	**1.49**
Dowtherm RP	−20	350	385	937	2007	0.115	1.32	1046	−0.738	1561	2.98
Dowtherm MX	−23	330	420	868	2032	0.109	0.96	981	−0.775	1545	3.25
Dowtherm 4000 (ethylene glycol—90% vol)	−30	177	–	1031	3138	0.269	0.62	1149	−0.753	2243	5.96
Syltherm 800	−60	400	385	820	1830	0.111	1.70	960	−0.978	1574	1.71
Syltherm XLT	−111	260	350	722	2045	0.080	0.34	876	−1.027	1730	2.10
Syltherm HF	−82	260	355	740	2002	0.075	0.43	892	−1.011	1633	2.46
Paratherm HR	−11	343	416	860	2200	0.107	0.93	965	−0.746	1884	2.30
Paratherm HE	3	310	371	781	2600	0.116	2.10	872	−0.611	1791	5.06
Paratherm GLT	8	288	n.a.	781	2500	0.110	1.30	887	−0.707	1929	3.60
Paratherm NF	−43	332	366	797	2500	0.098	1.50	899	−0.683	1469	7.97
Pirobloc mineral	−10	305	n.a.	782	2374	0.131	n.a.	879	−0.649	1811	3.72
Duratherm 450	−45	232	329	774	2473	0.133	0.77	876	−0.681	2021	3.02
Duratherm 600	−10	315	360	768	2336	0.136	2.01	869	−0.672	1844	3.27
Duratherm HTO	−15	315	360	758	2288	0.135	2.07	862	−0.665	1815	3.24
Duratherm S	−66	204	436	928	1926	0.117	0.98	968	−0.263	1641	1.91
Solar salt	220	600	–	–	–	–	–	2090	−0.636	1443	0.172
Hitec salt	142	535	–	–	–	–	18	2079	−0.732	–	–

where β_ρ and β_{cp} are the linear coefficients of the density and the specific heat capacity correlations respectively. From Table 16.4, it can be seen that organic heat carriers have lower thermal capacities, higher viscosities, and lower thermal conductivities than pressurized water. They are limited at high temperature because of stability issues due to their molecular structures, however, even at high temperature, they can often be operated at or near atmospheric pressure, creating cost savings and avoiding the mechanical hazards of high-pressure systems. Molten salts present a good thermal stability at high temperature and properties similar to water (high thermal capacity and conductivity, and low viscosity) at low vapor pressure. However, they are characterized by high-temperature melting-points (>150°C) which make them, in general, not suitable for ORC-based CSP systems.

Finally, besides thermophysical properties, the cost of the heat transfer carrier must be accounted in the design process of a solar power system. Price is function of the product quality, the seller, but also of the volume container. In the case of 200 L drums, cheap and low-grade HTFs are about 1−3 €/L, standard HTFs cost around 4−6 €/L, whereas high-grade fluids can cost up to 10−15 €/L.

16.2.3 Thermal energy storage

The intermittent nature of sunlight is an inherent drawback of solar power that can lead to imbalances between consumer demand and heat source availability. By adding energy storage, however, it is possible to shift excess energy from high-insolation periods to nighttime or periods of unfavorable meteorological conditions. The whole power system is thus more efficient (avoiding waste during periods where insolation outstrips demand), reliable (buffering system output during cloud passage), and flexible (higher capacity factor) despite transient external conditions. A key advantage of solar ORCs over photovoltaic technologies is the opportunity to use cost-effective thermal energy storage (TES), which stores excess heat energy in thermal rather than electrical form, in place of electrochemical batteries. TES, which is currently cheaper than commercial batteries and has a longer usable lifetime, comes in many varieties, and design/selection of the TES component of a SORC system must be undertaken with the following criteria in mind:

1. High energy density minimizes storage size;
2. High heat transfer rate permits fast storage and release of thermal energy;
3. Chemical compatibility is required between the storage medium, the container, and the HTF (if in direct contact);
4. High storage efficiency is needed over the complete charge−standby−discharge cycle; energy and exergy losses should be minimized;
5. Easy control and good flexibility;
6. Fluid selections should avoid environmental issues and limit hazards;
7. Lowest cost systems amplify advantage over electrochemical batteries.

Various TES technologies can be distinguished by the mechanism employed for storing heat energy, i.e. sensible, latent and chemical TES systems. These TES technologies are discussed in more detail in the following sections.

16.2.3.1 Sensible thermal energy storage

In sensible TES, heat storage is achieved by raising the temperature (without changing phase) of a single-phase medium. The amount of energy stored is proportional to the mass of the medium employed, its specific heat capacity, and the temperature difference between initial and final states. The storage material can either be the HTF flowing in the solar field (i.e., *direct* storage) or another medium (i.e., *indirect* storage). In the latter case, an additional heat exchanger is required to interface the SORC plant to the TES unit. Cost reductions for either direct or indirect storage can further be achieved by using inexpensive solid materials, preferably with high heat capacity, to partially fill the storage container (i.e., *packed-bed* TES). A list of common filler materials is given in Table 16.5.

Sensible TES can be integrated into SORC systems in three distinct architectures:

Single buffer

In this configuration a small volume capacity of HTF is placed in series with the solar loop (see Fig. 16.14). The buffer mitigates short fluctuations of temperatures at the outlet of the solar field (e.g., due to passing cloud cover). The storage capacity of the buffer tank is limited and is generally not used to extend operation of the SORC into nonsun periods.

Two-tank storage

Two-tank storage involves two separate reservoirs, which are used to store, respectively, hot and cold liquids (Fig. 16.15) in various system configurations. Two-tank

Table 16.5 Properties of potential solid filler materials for packed-bed storage (Kuravi et al., 2013; Singh et al., 2010; Grirate et al., 2013)

Filler material	Density (kg/m^3)	Heat capacity (J/kg K)	Conductivity (W/m K)	Thermal expansion (1e-5/K)
Concrete	2000–2400	750–900	0.4–1.5	2.5–4.5
Brick	1600–2000	850–1000	0.6–1.5	0.9–1.7
Basalt	2200–2800	800–1150	1.0–2.5	2.4–2.8
Granite	2500–2700	700–850	1.7–4.0	1.2–2.4
Limestone	2500–2800	830–1000	1.3–2.5	2.4–3.6
Marble	2600–2800	800–1150	2.0–3.0	1.7–3.6
Quartzite	2510–2860	700–1100	3.3–7.0	3.3–3.9
Sandstone	2100–2700	710–930	1.7–2.9	3.0–3.3
Aluminium	2700–2800	870–890	205–215	6.5–6.9
Cast iron	7200–7900	460–600	37–55	3.3–3.5
Steel	7750–7830	465–490	36–54	3.1–4.2

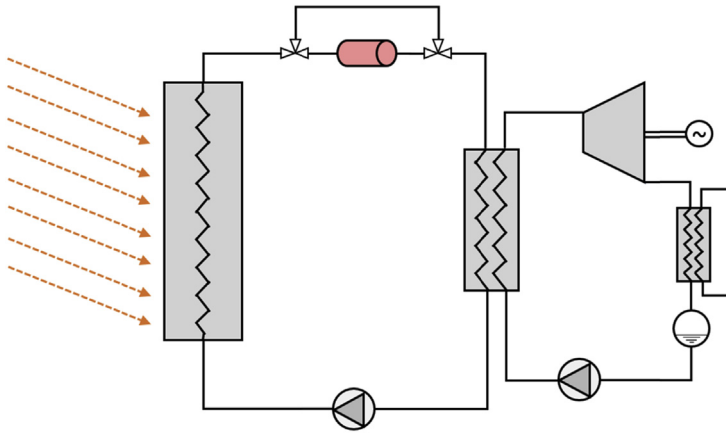

Figure 16.14 Buffer reservoir.

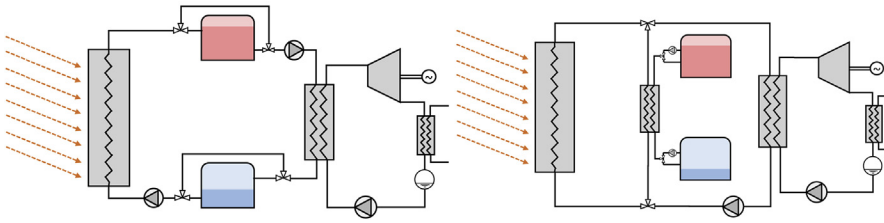

Figure 16.15 Direct (left) and indirect (right) two-tank thermal energy storage.

storage can have high thermal charge−discharge efficiencies (up to 95% if well insulated) and good operational flexibility. They are easily scalable and can be designed to widely extend the daily operational time of SORC by up to several hours.

Thermocline storage

As shown in Fig. 16.16, thermocline storage is a single tank used to store both hot and cold fluid where a natural separation is created by the density difference between the two zones of fluid. By using a single reservoir, cost reductions (up to 33% (Kolb, 2011)) can be achieved compared to two-tank storage, however, thermocline systems

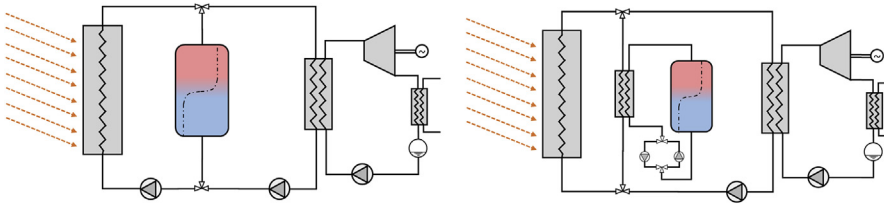

Figure 16.16 Direct (left) and indirect (right) thermocline storage.

are inherently less efficient than two-tank TES because of the imperfect separation between the hot and cold fluid. Thermal diffusion and mixing phenomena (e.g. turbulence due to flow) induce a transition zone of increasing thickness which degrades the high-temperature energy initially stored. In spite of this, thermocline TES is easily scalable and can be designed to extend the operational window of SORCs for many hours past sunset.

Overall, sensible heat storage is the most common TES technology used in SORC systems as it is simple, cost-effective, and has good heat transfer performance. However, the lower energy density ($\sim$kJ/m^3) implies large storage size compared to TES varieties discussed in Section 16.2.3.2.

16.2.3.2 Latent thermal energy storage

In this design, thermal energy is stored in the latent heat of a phase-change material (PCM). Since latent energy of phase-change transitions is much higher than specific heat capacity, PCM storage has the potential for much higher energy storage density ($\sim$MJ/m^3) than sensible TES. Among the different phase-change transitions possible, solid−liquid transitions are generally preferred because of the limited volumetric expansion of the storage medium during the process. Generally encapsulation of the storage media is required to avoid mixing between the liquid-phase PCMs and the HTF.

Another key advantage of latent storage is that the phase transition is a quasi-isothermal process, a feature that facilitates TES integration and control within the SORC plant. The tradeoff, however, is the low thermal conductivity of the storage media which results in an excessive charging and discharging time for thermal storage. Faster response times can be achieved by adding high-conductivity materials (e.g., metals or graphite) within the PCM.

Media for latent storage include organic materials (e.g., paraffins and fatty acids), inorganic compounds (e.g., salt hydrates), and various eutectic mixtures (see Table 16.6). Despite its technical advantages compared to sensible technologies, latent heat storage is more expensive and still at the prototype phase.

16.2.3.3 Thermochemical thermal energy storage

Thermochemical TES relies on reversible chemical reactions to store heat energy. In the charging process, injected heat is used to drive an endothermic chemical reaction; the chemical products are later used to restore thermal energy by performing the reverse (exothermic) reaction. Examples of potential materials for thermochemical storage in CSP are provided in Table 16.7. Among the different storage technologies, thermochemical TES has the highest energy density potential ($\sim$GJ/m^3) thanks to the large enthalpy change in chemical reactions. Additional advantages to thermochemical TES are quasi-isothermal storage and release, as well as storage of chemical products at ambient temperatures which largely reduces long-term thermal losses. Thermochemical storage is not yet mature, however, with high cost and technical complexity remaining barriers to commercialization.

Table 16.6 Examples of phase-change materials with their properties

Chemical formula	Medium name	Melting point (°C)	Density (kg/m^3)	Latent energy (kJ/kg)	Energy density (MJ/m^3)
$C_8H_8Cl_2$	p-Xylene dichloride	100	1432	139	199
$C_8H_8O_4$	Methyl fumarate	102	1370	242	332
$C_8H_4(OH)_2$	Catechol	104.3	1344	207	278
$C_6H_4O_2$	Quinone	115	1318	171	225
C_8H_9NO	Acetanilide	118.9	1219	222	271
$C_4H_4O_3$	Succinic anhydride	119	1230	204	251
C_6H_5COOH	Benzoic acid	121.7	1266	143	181
$C_{14}H_{12}$	Stibene	124	971	167	162
$C_6H_5CONH_2$	Benzamide	127.2	1341	169	227
$KNO_3 + NaNO_3$	-	222	2257	108	244
$NaNO_2$	Sodium nitrite	282	2168	212	460
$NaNO_3$	Sodium nitrate	310	2257	174	393
NaOH	Sodium hydroxide	318	2130	158	337
KNO_3	Potassium nitrate	337	2109	116	245
KOH	Potassium hydroxide	360	2100	167	351

Table 16.7 Examples of reactions for thermochemical storage

Chemical reaction	Temperature range (°C)	Energy density (GJ/m^3)
$FeCO_3 \leftrightarrow FeO + CO_2$	180−200	2.6
$CH_3OH \leftrightarrow CO + 2H_2$	200−250	−
$Ca(OH)_2 \leftrightarrow CaO + H_2O$	400−600	3
$CaCO_3 \leftrightarrow CaO + CO_2$	800−900	4.4
$6Mn_2O_3 \leftrightarrow 4Mn_3O_4 + O_2$	900−1000	1

16.3 Solar Organic Rankine Cycle systems

16.3.1 Design and specification

While there may be differences in the operating temperatures, working fluids, sizes and types of pumps, expanders, and heat exchangers for an SORC system, the fundamental methods for predicting the performance of a solar-integrated ORC system are similar to the thermodynamic modeling techniques described in Chapters 1, 6, and 7. The selection of cycle parameters optimized for a solar ORC, however, is driven mainly by the cost and temperature of the available heat source and cold reservoir (air in dry or wet cooling modes, or a local water body). In particular, the optimum operating temperature of a solar-driven ORC can vary with the type of collector (described in Section 16.2.1) and its relative efficiency as a function of temperature (efficiency decreases with increasing HCE temperature). This is a fundamental aspect of solar-integrated ORC systems; there is an opposing trend between efficiency and operating temperature for any solar collector (negative derivative) as compared to a thermodynamic cycle [positive derivative (efficiency increases with increasing expander inlet temperature)]. This implies that for any collector architecture, and taking into consideration the cooling strategy at the location of the plant, there is an optimum operating temperature where the tradeoff between collector and ORC efficiency is balanced to achieve the best overall plant efficiency.

16.3.2 Steady state performance prediction of solar ORC systems

A steady state model of a solar ORC describes an instantaneous snapshot of the state of the system. On a clear day sunlight impinges on a solar collector, photons are converted to thermal energy at an efficiency calculated from optical and material properties, thermal energy is then conveyed by an HTF at a prescribed flow rate to the evaporator of an ORC, where a working fluid reaches a two-phase, saturated, or superheated state at high pressure, and mechanical work is performed when the working fluid transits through the expander. Finally the high-volume, low-pressure working fluid is condensed, heat is rejected (to ambient air, water, or a secondary thermal loop in, for example, cogeneration), and power output from the expander/generator is divided by the amount of energy captured from the sun to calculate the efficiency. System performance is analyzed assuming that all environmental variables (solar insolation, ambient temperature, etc.) remain "constant enough" over a "long enough" period of time for their effects to propagate through the system (note that the deviation of actual conditions from these assumptions can be quantified to determine the extent of validity of steady state results). This conceptual framework provides the basis for simple models, discussed in this section, and even for complex models (e.g., dynamic models, as described in Section 16.3.3).

16.3.2.1 Solar collector modeling

To determine the performance of a solar collector (and therefore quantify the HTF temperature and energy content as supplied to the ORC) it is necessary to quantify the energy input:

$$\text{Energy in} = \text{DNI} * \text{aperture of the collector} * \cos\emptyset \tag{16.3}$$

(where $\emptyset$ is the angle of incidence) and a few other relevant parameters which affect the heat loss terms of the model, such as the temperature and mass flow rate of the HTF entering the collector, the ambient temperature and the wind speed. A typical solar collector model will calculate the fraction of sunlight energy lost via the following optical mechanisms:

- Cosine losses (as the sunlight impinges on the aperture at an angle of incidence theta, the actual power intercepted by the collectors is cos ϕ, and this can lead to further losses through "walk off" of the beam past the receiver end at the collector side furthest from the sun)
- absorption or scattering at the primary or secondary mirrors (reflective coefficient)
- missing the absorber target (intercept factor)
- shadowing of aperture area (by collector structures or nearby obstructions)
- absorption or scattering at any glass envelope
- reflection off of the absorber surface (inverse of absorbtivity)

After these losses are accounted for, the remaining energy is assumed to be absorbed as heat by the system, however, this heat does not entirely result in enthalpy gain of the HTF due to the inevitability of heat losses from the absorber. In typical solar collector models, such as the one developed by Forristall (2003), an energy balance is calculated on the HCE, taking into account its optical parameters (emissivity of absorber tube and glass glazing, if there is glazing), convection transfer at the HCE outer surface to air (as a function of ambient temperature and wind speed) and within any annulus (unless it is evacuated), and radiative losses propagating out from the absorber through any glazing. This involves a solution of the radial temperature distribution across the HCE (Fig. 16.17), taking into consideration conduction through any HCE materials and the heat transfer from the inner surface of the HCE to the HTF (as a function of the thermophysical properties of the HTF, e.g., thermal conductivity, heat capacity, viscosity, and velocity). Alternatively, empirical correlations can be used to derive the effective heat power absorbed by the fluid in function of the operating conditions (Dickes et al., 2015).

Such 1D energy balances may be performed on subsections of the HCE line and solved sequentially, where the output HTF temperature of the first node is used as the input HTF temperature for the second node, and so forth (Fig. 16.18). This method reproduces a temperature gradient along the absorber line, aggregates convection and radiation losses along the line, and estimates the outlet temperature and heat gain of the HTF, which is the relevant input parameter for the ORC model.

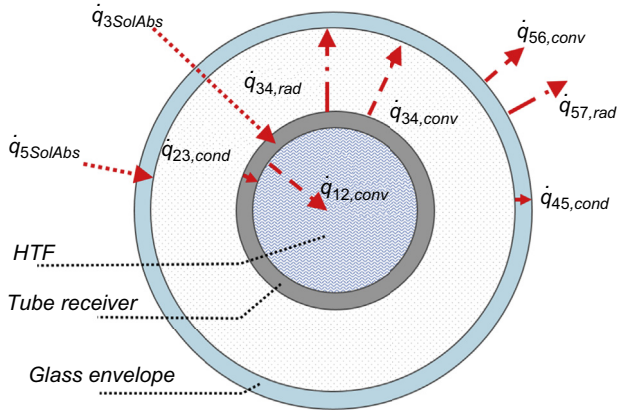

Figure 16.17 Radial temperature distribution across heat collection element boundaries beginning with the interface between the heat transfer fluid (HTF) and the inner diameter of the absorber (1-2), conduction across the absorber (2-3), radiation and convection from the outer diameter of the absorber to the inner diameter of the glass envelope (3-4), conduction across the glass envelope (4-5), and finally convection and radiation from the outer diameter of the glass envelope to the ambient air (5-6) and the sky (5-7) respectively.

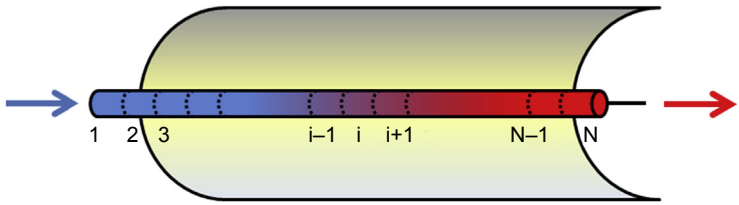

Figure 16.18 A 1D solution for energy balance is applied to sequential nodes with outlet temperatures of the nth node becoming the inlet temperature of the $n + 1$ node.

Note that the heat gain of the HTF (in Watts) divided by the original input term at the collector aperture, is the definition of solar collector efficiency:

$$\eta_{\text{col}} = \frac{\dot{m}\Delta h}{\text{DNI}\cdot A\cdot\cos\,\phi} \tag{16.4}$$

where ϕ is the angle of incidence of sunlight on the collector aperture.

Once the outlet temperature of the collector is known, it can be input into a detailed ORC model (iteratively, if the HTF inlet temperature of the solar loop is to be determined by the outlet temperature of the ORC vaporizer or preheater) or substituted into a simplified representation of a heat engine such as, e.g., a Chambadal-Novikov (De Parga, 2009) alternative to the Carnot efficiency approximating the operating experience of actual heat engines:

$$\eta_{\text{ORC}} = 1 - \sqrt{\frac{T_{\text{c}}}{T_{\text{h}}}} \tag{16.5}$$

where T_c and T_h are the hot source and cold sink temperatures, respectively.

The overall system efficiency is simply a product of these two component efficiencies (sunlight-to-heat and heat-to-power).

The drawback to this steady state approach lies in the assumption of steady or average DNI and average air temperature, whereas in reality these two driving parameters are constantly varying during normal operation of the ORC and "off-design" efficiencies may differ substantially from the average efficiency. At a minimum, the fluctuation in heat gain due to these changes frequently necessitates the use of thermal buffering, if not outright TES, to stabilize the inlet conditions at the ORC expander (as discussed previously). In order to consider the effects of thermal inertia (of the ORC, the collectors, or any buffering or storage components), it is necessary to make use of a dynamic modeling approach.

16.3.3 Dynamic performance prediction of solar organic Rankine cycles with thermal energy storage using typical meteorological year data

A thermal power plant operating from a constant heat source (such as a metered feedstock of combusting coal) is a good candidate for steady state calculations to determine typical performance parameters and specifications of major components, such as expanders and heat exchangers; in general, the system will always function at or very close to the steady state design point. A solar power plant, however, especially one that is expected to handle any load-following (such as an islanded solar microgrid), represents the opposite extreme; both energy delivery and demand will vary potentially quite far from the average values, and this points directly to the inadequacies of a steady state model.

For a solar ORC, the availability and intensity of sunlight is intermittent, and usually not synchronized with the variability in demand. If the operating temperature differential between source and sink is relatively small, as it tends to be with a solar ORC, fluctuations in ambient temperatures (and their dynamic with respect to heat availability) play a correspondingly larger role in the performance of the system.

Typical meteorological year or TMY datasets have been developed to standardize the characterization of such local fluctuations in ambient temperature and irradiance. These consist of historical weather observations for a set of 12 'typical' months, usually derived from a multiyear dataset, with hourly values. This type of data provides the baseline design conditions for engineering a system that can handle dynamics.

A parametric steady state approach to characterizing thermal power generation (solving steady state models for different ambient conditions) can lead to an understanding of off-design behavior, but only a dynamic model can lead to an understanding of which *nominal design*, given the certitude of continual *off-design* conditions, optimizes for the figure of merit (typically minimized total cost per unit of energy delivered). The following sections explain the motivation and approaches used to develop dynamic models to solve optimization problems for solar ORC systems.

16.3.3.1 Conservation of energy and thermal capacitance

Energy balance, or conservation of energy, is the principal framework for modeling power systems. At steady state, the sum of inputs and outputs is equal to zero for a power block. When energy inputs and outputs of a power system do not match for every point in time, the designer can smooth these discrepancies by introducing energy storage. Thus, a solar collector array can operate at its full output, without defocusing collectors, even when this heat flux exceeds the heat flux consumed by the ORC, or an ORC can operate at full output during a brief period of cloudy weather. The difference is simply enthalpy gain (or loss) in the TES component. Even if the available (sensible) TES temperature is declining (e.g., during operation after dusk), varying the HTF flow rate can maintain constant heat flux and evaporating temperature in the ORC as long as the temperature remains above an operating threshold.

In its most simple form, a dynamic solar ORC model extends the energy balance framework by adding mathematical terms for thermal capacitance. TES is generally the largest capacitance in the system, and its relation to other system components is inherently dynamic, as its role in the power system involves either charging or discharging energy while varying its internal energy (in practice, any TES is constantly discharging through heat leakage unless it reaches equilibrium with the surroundings). These transfers of energy happen in time, and consideration of the time discretization of a dynamic model is critical to avoid numerical diffusion type errors.

16.3.3.2 Selection of model timestep

Intuitively, if the residence time of a TES tank is 30 min, a 1 h timestep will fail to conserve and balance energy flows; energy storage calculations based only on initial and final temperatures will fail to account for the increase in temperature of the HTF volume that flowed into, and then out of, the TES tank during the timestep. If a solar collector field with a network of HCEs is used with an ORC, the change in solar collector outlet temperature for a step change in HTF inlet temperature will only manifest after the travel time in the collector (and will reach steady state, if nothing else changes, only after the thermal capacity of the HCEs have equilibrated). If the timestep is shorter than the travel time in a steady state solar collector model, energy conservation residuals will ensue, because within the timestep the gradient of temperatures from inlet to outlet is resolved, when in reality the collectors did not have enough time to propagate the change in inlet temperature all the way through to the outlet. This type of numerical diffusion error is framed by the Courant-Friedrichs-Lewy (CFL) condition, which holds that, in numerical simulations using finite difference methods, the time discretization must contain the analytical phenomenological domain influenced by the initial conditions (Courant et al., 1967). Selection of an appropriate timestep as a function of the spatial discretization of components in Solar ORC dynamic simulation meeting the CFL condition can thus include:

$$\frac{\text{thermal capacity}(\text{J})}{\text{thermal power}(\text{J/s})} > \text{timestep} < \frac{L_{\text{HCE}}(\text{m})}{v_{\text{HTF}}(\text{m/s})} \tag{16.6}$$

(the second boundary above the timestep could be eliminated by the use of a dynamic solar collector model, similar to the approach taken with a TES tank). Other conditions, for example, volumes and flow rates in tanks, may be considered as well, but in general the consideration of dynamic simulation timestep involves the tradeoff between impractical computational effort at infinitesimal timesteps and numerical failure to converge at timesteps too large to meet the CFL condition.

16.3.3.3 Control strategy

The dynamic simulation of a solar ORC requires definition of control parameters and strategies (defining initial and operational modes), and presents an opportunity to optimize these in software before implementing them in practice. In a dynamic solar ORC simulation, the various components, including TES, are connected to each other via mass and energy flows, which may in turn depend on external conditions. Once the operational modes have been defined (e.g., by system temperatures or pressures, or by external conditions), conditional statements can be used with parameter threshold values to trigger selection between modes based on conditions for the given timestep.

The major controllable variables in a solar ORC are the flow rates of the HTF and the working fluid, the speed of the cooling fan/pump, the tracking of the collectors (on/off), and the setpoint of the expander rotational speed. Various scenarios with different operating setpoints for these components can be articulated, with real time acquisition of sensor data triggering the shift from one operational mode to another in the operation of a real system (and conditional statements embodying this behavior in the dynamic simulation).

The number of unique modes and parameter combinations triggering mode shifts are too extensive and application specific to describe comprehensively, but a few examples are given here for illustration.

Typical startup sequence

- When DNI reaches a certain threshold (e.g., 200 W/m^2), solar collectors are set to tracking mode
- When temperature in the absorber of the solar collector reaches a certain threshold (depending on the application) HTF flow is initiated
- When temperature of the HTF entering the ORC vaporizer (potentially supplied from TES) reaches a certain threshold, the ORC is engaged, i.e., working fluid pump (and potentially expander variable frequency drive) and condenser cooling fan/pump are activated

Example operational considerations

- To maintain the design pressure ratio across the expander, the HTF flow rate and condenser heat rejection rate may be modulated on the basis of, for example, degrees of working fluid superheat at the expander inlet or temperature pinch in the condenser
- In the event of a cloud passing or dusk (DNI lower threshold being reached), the HTF flow in the collector field may be stopped to avoid rejecting heat at the CSP HCE, while HTF flow in the TES−ORC loop may be maintained for continuous power output (provided sufficient HTF temperature, above a set threshold, is available from the TES).

Operational systems may be shut down normally (according to a reverse of the above sequence) or due to some perturbation such as a cloud passing, low temperature in the HTF loop, or error states such as locked rotors, cavitation in the working fluid pump, excessively high temperature, etc. One specialized case of exceptional shutdown that can be easily diagnosed is frequent defocusing of a solar field due to overtemperature conditions; generally this points to an undersizing of the TES and/or the ORC components relative to the solar field in the system design.

The various thresholds deployed in the control system and the modes associated with various combinations of sensor inputs are themselves also subject to dynamic optimization. For example, Ireland et al. (2014) performed a parametric sweep of HTF temperature thresholds for engaging an ORC and found that system performance (in dynamic simulation of a solar ORC with TES) is highest when the ORC is only turned on when approaching the maximum allowable HTF temperature, as opposed to the minimum viable HTF temperature or some intermediate value (Ireland et al., 2014). Mitterhofer and Orosz (2015) conducted a parametric sweep of condenser size, temperature defect, and pressure ratios in a dynamic simulation of a pilot 3 kW_e solar ORC (installed by STG International at Eckerd College in St. Petersburg, FL) to identify optimum expander volume ratio, condenser size, temperature defect, and coolant fan effort setpoints for variable ambient temperatures, using TMY data and levelized cost as an objective function (Mitterhofer and Orosz, 2015). Observations from this study included the cost advantages of using smaller air cooled condensers with a higher temperature defect in the ORC cycle; the efficiency gains from a large condenser are outweighed by the relative expense of this component.

Because of the specificity of ambient climate conditions and project purpose and sizes, results from such studies, while informative, are typically not generalizable, and detailed analysis are required to identify optimized control strategies, operational modes, and threshold variables for each application. Furthermore, even for a given technology design, control strategies and threshold variables must be validated independently for the particular load profile and meteorological conditions experienced at each new deployment location.

16.3.4 Solar Organic Rankine Cycle optimization and economics

A physics-based representation of a solar ORC with thermal capacitance is essential for accurate prediction of performance and sizing of components. While performance and efficiency are influential metrics, several other factors may bear on the design of the system, as conceived in the context of a real-world application. The decision to deploy solar collectors with an ORC (and potentially TES) and determining appropriate sizing amongst the components, will usually be made only after evaluating specific project criteria; cost effectiveness compared to alternative options usually being foremost among them. The analysis of performance and cost of various configurations necessarily entails design engineering of the system for the particular application which, to the extent that applications vary widely and are sited across a range of locations with unique irradiance and climate characteristics, poses both a technical and economic challenge (cost of engineering

hours, time required to complete designs and dynamic simulations, etc.). These challenges have undoubtedly limited the deployment of solar ORCs historically.

16.3.5 Application engineering and system analysis

Many variables impact solar ORC project design, and it can be difficult to know where to start because the most important factors may be different in each individual case. The following list of considerations is neither comprehensive nor necessarily in order of priority but can provide a starting point for conducting a prefeasibility analysis. Before engaging in a solar ORC project, relevant information to gather can include:

- What is the location of the application? With this known, the closest station with TMY data can be used to characterize the available irradiance and ambient temperature patterns.
- What is the shape and variability of the load profile? What is the peak load (kW), total daily load (kWh), and variability in load throughout the day? What is the form of the load to be supplied (i.e., are there both thermal and electrical loads)? Is a profile of the demand well constrained in the time domain across major operating modes? Is thermal demand in the form of process or building heating, or does it require cooling? What are the target heating or cooling temperatures? Is there seasonality to the load? These data are critical for accurately parameterizing a dynamic simulation of the system and assessing the need for TES.
- Is there integration with any other thermal source (e.g., biomass, fossil fuel, geothermal, waste heat, etc), and if so, what is the capacity, availability, and cost of the alternative source? These data will influence the relative sizing of both the solar component and TES and will drive overall project economics.
- Given the temperatures involved, what type of solar collector, HTF, and ORC working fluid are most suitable?
- Given the size of the application and availability of expander−generator packages, which expander type (positive displacement or turbomachine) is suitable?
- Is the type of heat rejection (dry, wet, or water) constrained (e.g., lack of available water in desert regions), or will the decision be made on a least cost basis?
- What is the source of project finance and what are the terms, e.g., for debt financing what would be the loan tenure and interest rate?
- What is the market value of the system outputs?
- What standard alternative systems (gas burners, heat pumps, PV and battery systems, etc.) are available for the application, and what would be the total cost of deploying a competing technology?

These data and others specific to the project will inform the decision process for whether a solar ORC is an economically viable option and will guide the modeling process for deciding how to implement a solar ORC or hybrid system.

16.3.5.1 Design of Organic Rankine Cycle systems for use with solar collectors

Once the temperature regime of the system is determined, the next important specification is the selection of an ORC working fluid, which influences the expander configuration via the pressure−volume ratio of the ORC and the size of heat exchangers for thermal input and heat rejection. In a parametric study of solar ORC performance and

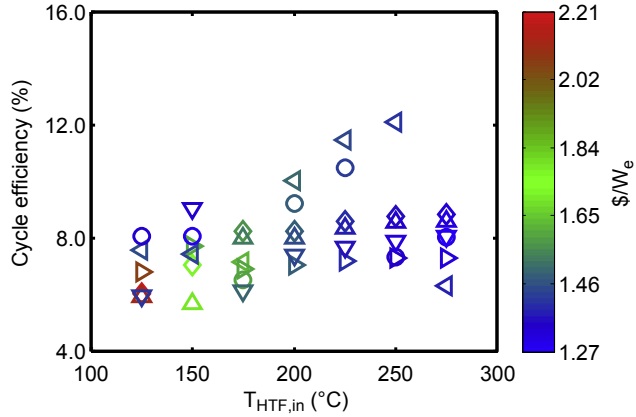

Figure 16.19 Specific cost ($/$W_e$) and cycle efficiency for various working fluids evaluated at heat transfer fluid (HTF) inlet temperatures from 125 to 275°C for a 5 kW_e Organic Rankine Cycle. △, butane; ▷, isobutane; ◁, R134a; ○, R161; ▽, R152a (Garg et al., 2015).

economics, Garg et al. (2015) investigated the specific costs of power for 16 zero-Ozone Depletion Potential (ODP) and positive condenser pressure (saturation pressure corresponding to 45°C) working fluids for HTF supply temperatures between 125 and 275°C (the top five most cost efficient fluids are shown in Fig. 16.19). This analysis showed that specific costs of electricity between 1.25 and 2 USD/W are achievable for optimized solar ORC systems using a parabolic trough solar collector, with cost advantages at increasing operating temperatures (Garg et al., 2015). Note that a significant result of this study is that cost efficiency and thermodynamic efficiency are not necessarily correlated when decisions, for example, to recuperate or not and variable condenser size/fan duty are optimized for cost.

16.3.6 Specific and levelized costs of power generation

Solar ORCs have historically been developed more often for research and demonstration purposes than for commercial applications. Where the decision to deploy depends on market forces, various financial metrics such as internal rate of return (IRR), payback period, total cost of ownership, discounted cash flow, etc., may be selected as a figure of merit for a project developer. To varying degrees, poor economic performance coupled with the necessity for complex dynamic simulation to arrive at calculated performance and optimized cost configurations may account for the scarcity of commercial solar ORC installations to date.

Specific capital costs for a nominal power output are relatively straightforward to calculate and compare among alternatives when the output is electrons (i.e., $/W) but may be more difficult to assess or present in a simple metric, when the outputs are combined heat and power. Even for electricity, $/W for solar plants is typically indicated in peak Watts ($/$W_{peak}$), whereas the daily energy generated by an equivalent nameplate capacity system could vary significantly between, for example, fixed tilt PV systems and tracking CSP systems due to the latter's higher production levels in the

morning and evening. Levelized energy costs can be calculated by dividing capital plus operating and maintenance costs by the total amount of energy produced (estimated via simulation methods), though this too is generally more useful for electricity than for thermal outputs and is difficult to assess in scenarios where the value of outputs changes (such as with time-of-use pricing for electricity).

If the objective of the project is to maximize IRR for a given amount of investment through the sale of electricity to a single off-taker, the evaluation of the project would utilize different metrics than in the case of, say, an industrial microgrid with cogeneration. In the former project, the use of storage and dynamics of time-of-use pricing would be important considerations, while in the latter the evaluation framework could be minimizing the total cost of ownership or comparison against the status quo alternative, which is likely to have a well-known cost. Projects that are designed to maximize profit through sale of energy as a commodity are therefore conceptually different from projects where the objective is to meet a particular energy demand profile at minimized cost.

Where cost minimization for a particular demand curve is sought, a general figure of merit is the net present cost (NPC) (Orosz et al., 2013):

$$\mathrm{NPC} = I_{\mathrm{o}} + \sum_{t=0}^{n} \frac{O_t + M_t}{(1+r)^t} \tag{16.7}$$

where I_{o} is the initial cost of the equipment, n is the service life in years, O_t and M_t represent Operating and Maintenance costs in year t, and r is the discount rate (Guth, 2009). Operating cost (O_t) is a unique function of the technology (e.g., fuel consumption) while maintenance cost (M_t) can be generalized as a function of the initial costs in two terms: a constant annual service component and a linearly increasing component for repairs due to wear with age, as shown in Eq. (16.8).

$$M_t = \frac{f}{n} + \frac{f \cdot (1-a)}{n^2} \cdot (2t-1) \tag{16.8}$$

where f is the fraction of total maintenance costs with respect to initial costs, and a is a coefficient expressing the fraction of regular service costs with respect to total maintenance costs (including incremental repairs). Various values for these coefficients can be found in the literature or in manufacturers manuals and maintenance procedures (NREL, 2013).

For demand driven projects, NPC is a valuable tool for comparison between alternative energy system configurations serving the same purpose, but other figures of merit may be preferable depending on the planner's objectives and type of available finance and the target applications of the system.

16.3.7 Optimization tools

Once a figure of merit (typically economic) is selected, the process for optimizing according to this metric involves varying system level approaches (solar ORC or

some competing solution), components, configurations, control strategies, etc., while evaluating the systems against the application conditions and known dynamics (DNI, ambient temperature, demand, and possibly time-of-use pricing). The calculation for the economic figure of merit is added to the already complex dynamic simulation of energy flows in a solar ORC or hybrid system, and in most cases an exhaustive search of the inherently irregular parameter space will be prohibitively expensive/slow to compute even using multicore cloud computing resources. This motivates the use of optimization algorithms, a diverse and specialized set of tools that can achieve maximization or minimization of an objective function with drastically reduced computational effort.

The various approaches, described in more detail in Chapter 7, include evolutionary and gradient methods, among others. The genetic algorithm (GA), inspired by biological evolution, "breeds" a population of ever more optimized solutions through successive generations, escaping the local maxima or minima that can trap gradient-ascent ("hill-climbing") methods via "mutations" that sample more widely in the search space. Particle swarm optimization (PSO) similarly employs a population of solutions, with the candidates initially dispersed and the vector of the "swarm" in the search space is parametrically updated to move towards the "leader" (optimum metric for a given search timestep) without reference to any evolutionary operators such as "breeding", "crossover", or "mutation." Once the leader is established in the monotonic region of the global optimum, the optimization can drop the swarm and switch to a faster gradient-ascent/descent from the leader's position, however, this requires either some understanding of the search space or a metric for identification of the globally optimum 'hill.' GA and PSO, as well as more traditional gradient methods, can be applied to solar ORC optimization to greatly reduce computation time; for deeper analysis into their relative benefits the reader is referred to the literature (Hassan et al., 2004).

16.3.8 Case study: hybrid solar Organic Rankine Cycle microgrid system

While the recent advent of inexpensive crystalline silicon PV panels may have undermined the economic rationale for standalone solar ORC systems, viable applications for the technology exist in niches created by the need for storage, the utility of cogeneration, and the availability of inexpensive alternative supplies of thermal energy. One scenario that can meet these conditions is the deployment of a solar ORC within an isolated, hybrid microgrid consisting of PV and fossil fueled backup generation, and serving community combined heat and power loads (Fig. 16.20).

While renewable energy technologies are preferable for many reasons (long-term sustainability, emissions reductions, and even price considerations in extremely rural locations), to achieve 100% availability (capacity factor near to 1) in such a system with only PV panels and without ever resorting to a backup generator would be prohibitively expensive under the current price structure of deep cycle batteries (>250 USD/kWh). The addition of a solar ORC with TES can reduce (though not fully eliminate) the need for battery storage, but may only be economically justified in cases where a second

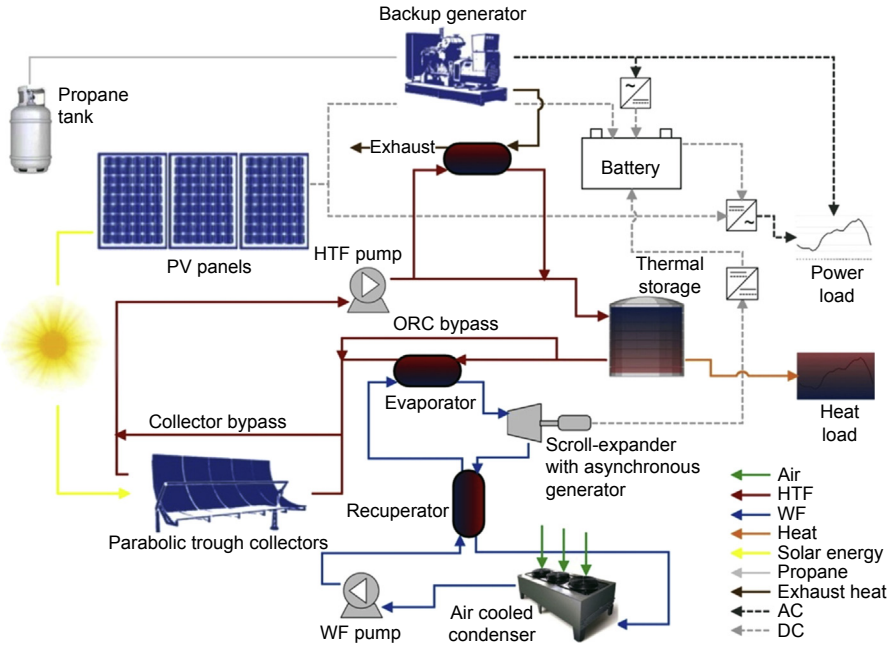

Figure 16.20 Hybrid Microgrid including photovoltaic (PV), concentrating solar power (CSP), Organic Rankine Cycle (ORC), thermal energy storage (TES), and a backup generator using liquefied petroleum gas (LPG).
Adapted from Mitterhofer, M., Orosz, M., 2015. Dynamic simulation and optimization of an experimental micro-CSP power plant. PowerEnergy. doi:10.1115/ES2015-49333.

use of the solar heat is specified, such as for heating institutions or dormitories. The need for a reciprocating internal combustion engine generating set to ensure high availability, however, also provides an opportunity for waste heat recovery from the approximately 60% of the fuel exergy that leaves with the exhaust (Teng and Regner, 2006). Note that while an optimum operating temperature for the ORC can be found for a given location and solar collector type (discussed in Section 16.3.1), the introduction of a second heat stream may influence the optimum operating temperature of the hybrid system due to the tradeoffs involved with a second heat exchanger and the temperature of the waste heat stream, driving the need to simulate the entire system simultaneously.

Definition of loads for a new hybrid microgrid could be derived from a survey and inventory method to predict energy consumption, but a more reliable approach would be to produce a probabilistic distribution function from a dataset of measured loads at comparable communities (i.e., ones which were only recently connected to the grid and have similar size and economic activity levels) (Orosz and Mueller, 2015). For institutional thermal loads, a building envelope model such as developed under Annex C of ISO 13790 (2008) could be parameterized for the structure of interest and exercised in dynamic simulation with local TMY data to produce a time distribution of thermal demand. Once the load profiles are established with reasonable granularity

(hourly or better), dynamic simulation of the hybrid microgrid can be performed where the allocation of PV panels, batteries, CSP collectors, and TES can be varied parametrically through an optimization method (such as PSO) within a control framework for prioritizing energy flows between components and to the load. A simple example framework for this application would be:

1. While the sun is shining, the load is supplied (via inverter) from the PV directly to the extent that PV power is sufficient to cover the load
2. If the PV power is insufficient to meet the load, the load is supplied from a battery bank (via inverter), as long as the battery storage is not depleted
3. If the PV power exceeds the load, the excess energy charges the battery bank
4. While the sun is shining the CSP collectors charge the TES, until the TES capacity is reached
5. Thermal loads are supplied by discharging the TES
6. If the TES is insufficient to supply the thermal load, a backup (fueled) source is engaged for heat production
7. If TES reaches overtemperature limits, the ORC is engaged to convert heat to electricity (except in case 9 below)
8. If the ORC is engaged while the PV is supplying power, its effect is to augment the PV power and conforms to 2 and 3 (above)
9. If the battery bank reaches a full state of charge (SOC) while PV power and/or ORC power is exceeding the load, the excess PV power is directed to a load dump or sections of the array are open circuited, and the ORC is disengaged
10. If the TES reaches overtemperature limits while case 9 holds, the CSP collectors are defocused
11. If the battery reaches a low SOC threshold while the TES is charged, the ORC is engaged
12. If the battery reaches a lowest SOC threshold while the TES is discharged and there is no PV power, the backup generator is engaged
13. If the generator is engaged and the battery state of charge or the TES SOC reaches a (design point) recharge threshold, the generator is disengaged.
14. If the generator is engaged and the sun resumes shining, the generator is disengaged (to preserve battery capacity for the solar systems).

Other special cases can be envisioned but the above is an outline of a simple hierarchy of power flows that can be considered when sizing and optimizing a hybrid microgrid and implementing its control strategy.

A one year simulation is likely to be sufficient for extrapolation across the project lifetime, as a multiyear simulation would not produce results significantly different enough to justify the additional computational effort. The annual simulation would proceed with load and TMY input at each timestep, track the SOC of the storage components, and track the cumulative fuel usage in the backup generator (which constitutes the operating cost), all while ensuring that the demand (at each timestep) is met.

If the objective function of the microgrid simulation is determination of the minimized cost-recovery tariff for electricity and heat, then for a given combination of load dynamic and location there will be some configuration of the PV, battery, CSP, TES, and ORC components that is optimum (note that under some circumstances this could be a size of zero for a particular component). When performing the optimization, it is useful to set boundaries for the parameter space to be explored, i.e., whereas the generator is sized to meet the peak load with a factor of safety, the PV

or ORC components might be varied parametrically from zero to some multiple of the peak load (not more than 5). The battery and TES components could likewise be varied from zero to some multiple of an average day's energy requirements, calculated from integrating the load profile (not more than 3).

The cost functions of all components and the financial terms of the project finance (loan tenure and interest) being known, the objective function of minimized cost-recovery tariff can be solved for with an optimization algorithm searching the tariff space in a project lifetime cash flow model accounting for initial and recurring costs: operations, maintenance, loan repayment, and battery replacement (a function of battery type and the number of charge cycles which is tracked in the dynamic simulation). Identification of the cost minimizing solution enables one to proceed with specific component selection and provides a foundation for sizing and engineering design of the microgrid. To date, the case study just described has not been realized, and therefore validation of the simulation and hybrid design approach awaits future research and piloting programs.

References

Ait-Baha CSP Pilot Plant - Technical Datasheet.

American Inventor Uses Egypt's Sun for Power, July 2, 1916. Appliance Concentrates the Heat Rays and Produces Steam. New York Times.

ASTM, 2012. Standard tables for reference solar spectral irradiances: direct normal and hemispherical on 37° tilted surface. ASTM 1−21.

Bado, G., Tomei, G., Angelino, T., Gaia, M., Macchi, E., 1979. The Ansaldo 35 kW solar power system. In: Proceedings of the Silver Jubilee Congress, pp. 1090−1094.

Baral, S., Kim, D., Yun, E., Kim, K., 2015. Experimental and thermoeconomic analysis of small-scale solar organic rankine cycle (SORC) system. Entropy 17 (4), 2039−2061.

Barutti, A., Pedrick, W.G., Angelino, G., Gaia, M., Macchi, E., 1984. Ansaldo solar thermal and photovoltaic plants located at Ballajura, western Australia. In: Proceedings of the 8th Solar World Congress 1983, Biennial Congress of the International Solar Energy Society, vol. 3, pp. 1572−1576.

Bronicki, L., 2013. Short review of the long history of ORC power systems. In: ASME ORC13.

Canada, S., Brosseau, D., Kolb, G., Moore, L., Cable, R., Price, H., 2005a. Status of APS 1-Mwe parabolic trough project. In: 2005 DOE Solar Energy Technologies.

Canada, S., Cohen, G., Cable, R., Brosseau, D., Price, H., 2005b. Parabolic Trough Organic Rankine Cycle Solar Power Plant NREL CP/-550-37077. Denver, CO.

Chambers, T., Raush, J., Russo, B., 2014. Installation and operation of parabolic trough organic rankine cycle solar thermal power plant in south Louisiana. Energy Procedia 49, 1107−1116.

Courant, R., Friedrichs, K., Lewy, H., March, 1967. On the partial difference equations of mathematical physics. IBM Journal 11.

De Parga, G.A., 2009. The Curzon-Ahlborn Efficiency for Three Different Energy Converters, vol. 1, pp. 1−4.

Delgado-Torres, A.M., García-Rodríguez, L., October 2007. Comparison of solar technologies for driving a desalination system by means of an organic Rankine cycle. Desalination 216 (1−3), 276−291.

Dfid, 2010. A potential role for an AMC in supporting dish/Stirling concentrating solar power, case study annex. Advance Market Commitments for Low-carbon Development. http://www.vivideconomics.com/wp-content/uploads/2010/03/Micro_CSP_case_study.pdf.

Dickes, R., Dumont, O., Declaye, S., Quoilin, S., Bell, I., 2014. Experimental investigation of an ORC system for a micro-solar power plant. In: Proceedings of the Purdue Conferences 2014.

Dickes, R., Lemort, V., Quoilin, S., 2015. Semi-empirical correlation to model heat losses along solar parabolic trough collectors. In: Proceedings of ECOS 2015.

Duffie, J.A., Beckman, W.A., Worek, W.M., 1994. Solar Engineering of Thermal Processes, second ed. Wiley.

Dumont, O., Quoilin, S., Lemort, V., June 2015. Experimental investigation of a reversible heat pump/organic Rankine cycle unit designed to be coupled with a passive house to get a Net Zero Energy Building. International Journal of Refrigeration 54, 190–203.

Einav, A., 2004. Solar energy research and development achievements in Israel and their practical significance. Journal of Solar Energy Engineering 126 (3), 921.

Electratherm METU NCC Solar ORC Report. Electratherm Website, 2010.

Fenton, D.L., Abernathy, G.H., Krivokapich, G.A., Otts, J.V., 1984. Operation and evaluation of the Willard solar thermal power irrigation system. Solar Energy 32 (6), 735–751.

Forristall, R., 2003. Heat Transfer Analysis and Modeling of a Parabolic Trough Solar Receiver Implemented in Engineering Equation Solver. Golden, CO.

Galvez, J.B., 2010. Powersol: Mechanical Power Generation Based on Solar Thermodynamic Engines - Final Report.

Garg, P., Orosz, M.S., Kumar, P., Dutta, P., 2015. Thermo-economic Evaluation of ORCs for Various Working Fluids, pp. 1–16.

Georges, E., Declaye, S., Dumont, O., Quoilin, S., Lemort, V., 2013. Design of a small-scale organic rankine cycle engine used in a solar power plant. International Journal of Low-Carbon Technologies 8 (Suppl. 1), 1–8.

Goswami, D.Y., Stefaakos, E., Rahman, M.M., Aydin, S., Reedy, R., 2013. Design, Construction and Operation of CSP Solar Thermal Power Plants in Florida.

Grirate, H., Zari, N., Elamrani, I., Couturier, R., Elmchaouri, A., Belcadi, S., Tochon, P., 2013. Characterization of several Moroccan rocks used as filler material for thermal energy storage in CSP power plants. Energy Procedia 49, 810–819.

Guth, J.H., 2009. Resolving the Paradoxes of Discounting in Environmental Decisions, vol. 2008, pp. 95–114.

Hassan, R., Cohanim, B., de Weck, O., Venter, G., 2004. A comparison of particle swarm optimization and the genetic algorithm. American Institute of Aeronautics and Astronautics 1–13.

Helwa, N.H., Bahgat, A.B.G., El Shafee, A.M.R., El Shenawy, E.T., Bahgat, A.B.G., El Shafee, A.M.R., El Shenawy, E.T., November 2000. Maximum collectable solar energy by different solar tracking systems maximum collectable solar energy by different solar tracking systems. Energy Sources 22.

ISO 13790:2008 Energy performance of buildings – Calculation of energy use for space heating and cooling.

Ireland, M., Orosz, M., Brisson, J., Desideri, A., Quoilin, S., 2014. Dynamic modeling and control system definition for a micro-CSP plant coupled with thermal storage unit. In: ASME Turbo Expo 2014: Turbine Technical Conference and Exposition GT2014-27132.

Kalogirou, S.A., 2004. Solar thermal collectors and applications. Progress in Energy and Combustion Science 30 (3), 231–295.

Kane, M., Larrain, D., Favrat, D., Allani, Y., 2003. Small hybrid solar power system. Energy 28 (14), 1427–1443.

Kiceniuk, T., 1985. Development of an Organic Rankine-Cycle Power Module for a Small Community.

Kohlenbach, P., Mcevoy, S., Stein, W., Burton, A., Wong, K., Lovegrove, K., Burgess, G., Joe, W., Coventry, J., 2006. A new parabolic trough solar collector. In: Australian and New Zealand Solar Energy Society, pp. 1−8.

Kolb, G.J., 2011. Evaluation of annual performance of 2-Tank and thermocline thermal storage systems for trough plants. Journal of Solar Energy Engineering 133 (3).

Kuravi, S., Trahan, J., Goswami, D.Y., Rahman, M.M., Stefanakos, E.K., 2013. Thermal energy storage technologies and systems for concentrating solar power plants. Progress in Energy and Combustion Science 39 (4), 285−319.

Lovegrove, K., Stein, W., 2012. Concentrating Solar Power Technology - Principle, Developments and Application. Woodhead Publishing.

Manolakos, D., Papadakis, G., Kyritsis, S., Bouzianas, K., February 2007. Experimental evaluation of an autonomous low-temperature solar Rankine cycle system for reverse osmosis desalination. Desalination 203 (1−3), 366−374.

Mitterhofer, M., Orosz, M., 2015. Dynamic simulation and optimization of an experimental micro-CSP power plant. PowerEnergy. http://dx.doi.org/10.1115/ES2015-49333.

Moustafa, S., Hoefler, W., El-Mansy, H., Kamal, A., Jarrar, D., Hoppman, H., Zewen, H., 1984. Design specifications and application of a 100 kWe (700 kWth) cogeneration solar power plant. Solar Energy 32 (2), 263−269.

Mueller, A., Orosz, M., Kumar Narasimhan, A., Kamal, R., Hemond, H., Goswami, Y., 2016. Evolution and feasibility of decentralized concentrating solar thermal power systems for modern energy access in rural areas. MRS Energy Sustainability 3.

N'Tsoukpoe, K.E., Azoumah, K.Y., Clerc, E., Zmuda, J., Gaye, M., Seshie, Y.M., Kenda Nitedem, S.E., 2014. CSP4Africa : développement d'un pilote économiquement viable d'une mini-CSP pour la production d'électricité pour mini-réseau en Afrique.

NREL, 2013. "Distributed Generation Renewable Energy Estimate of Costs (Online). Available: http://www.nrel.gov/analysis/tech_lcoe_re_cost_est.html.

NREL - CSP Projects Review.

Orosz, M., Mueller, A., 2015. Dynamic simulation of performance and cost of hybrid PV-CSP-LPG generator micro grids with applications to remote communities. In: ASME Power & Energy Conference 2015.

Orosz, M.S., Quoilin, S., Hemond, H., 2013. Technologies for heating, cooling and powering rural health facilities in sub-Saharan Africa. Proceedings of The Institution of Mechanical Engineers Part A-journal of Powerand Energy 227 (7), 717−726.

Orosz, M.S., 2012. Thermosolar and Photovoltaic Hybridization for Small Scale Distributed Generation: Application for Powering Rural Health. Massachusetts Institute of Technology.

Orosz, M., 2015. Photovoltaics and concentrating solar power: why hybridization makes sense. SPIE Newsroom 1−4.

Pytilinski, J.T., 1978. Solar energy installations for pumping irrigation water. Solar Energy 21 (4), 255−262.

Reda, I., Andreas, A., 2008. Solar Position Algorithm for Solar Radiation Applications.

Rieu, V., September 2012. A 10 kW solar power plant for rural electrification. In: Proceedings of SolarPACES 2012.

Saitoh, T., Yamada, N., Wakashima, S., 2007. Solar Rankine cycle system using scroll expander. Journal of Environmental Engineering 2 (4), 708−719.

Simonnot, G., Louche, A., Decanini, Y., 1987. Three years exploitation of the 100 kWe Ajaccio solar power plant. In: Proceedings of the ISES Solar World Congress, pp. 1588−1592.

Singh, H., Saini, R.P., Saini, J.S., 2010. A review on packed bed solar energy storage systems. Renewable & Sustainable Energy 14 (3), 1059−1069.

Tabor, H.Z., Doron, B., 1990. The Beith Ha'Arava 5 MW(e) Solar Pond Power Plant (SPPP)—Progress report. Solar Energy 45 (4), 247−253.

Tabor, H., 1981. Solar ponds. Solar Energy 27 (3), 181−194.

Tchanche, B.F., Lambrinos, G., Frangoudakis, a., Papadakis, G., April 2010. Exergy analysis of micro-organic Rankine power cycles for a small scale solar driven reverse osmosis desalination system. Applied Energy 87 (4), 1295−1306.

Teng, H., Regner, G., 2006. Achieving high engine efficiency for heavy-duty diesel engines by waste heat recovery using supercritical organic-fluid Rankine cycle. In: SAE Pap., No. 724.

Thakur, D., 2013. A case study on the solar biomass hybrid distributed power generation project at Shive village. In: Odisha Solar Conference.

Wang, X.D., Zhao, L., Wang, J.L., Zhang, W.Z., Zhao, X.Z., Wu, W., March 2010. Performance evaluation of a low-temperature solar Rankine cycle system utilizing R245fa. Solar Energy 84 (3), 353−364.

Wang, X.D., Zhao, L., Wang, J.L., 2011. Experimental investigation on the low-temperature solar Rankine cycle system using R245fa. Energy Conversation and Management 52 (2), 946−952.

Weinrebe, 2007. Renewable energy - technology, economics and environment. In: Solar Thermal Power Plants (Chapter 5).

Zhang, S., Wu, Z.H., Zhao, R.D., Yu, G.Y., Dai, W., Luo, E.C., 2014. Study on a basic unit of a double-acting thermoacoustic heat engine used for dish solar power. Energy Conversation and Management 85, 718−726.